Neuron

Brain-derived autophagosome profiling reveals the engulfment of nucleoid-enriched mitochondrial fragments by basal autophagy in neurons

Graphical abstract

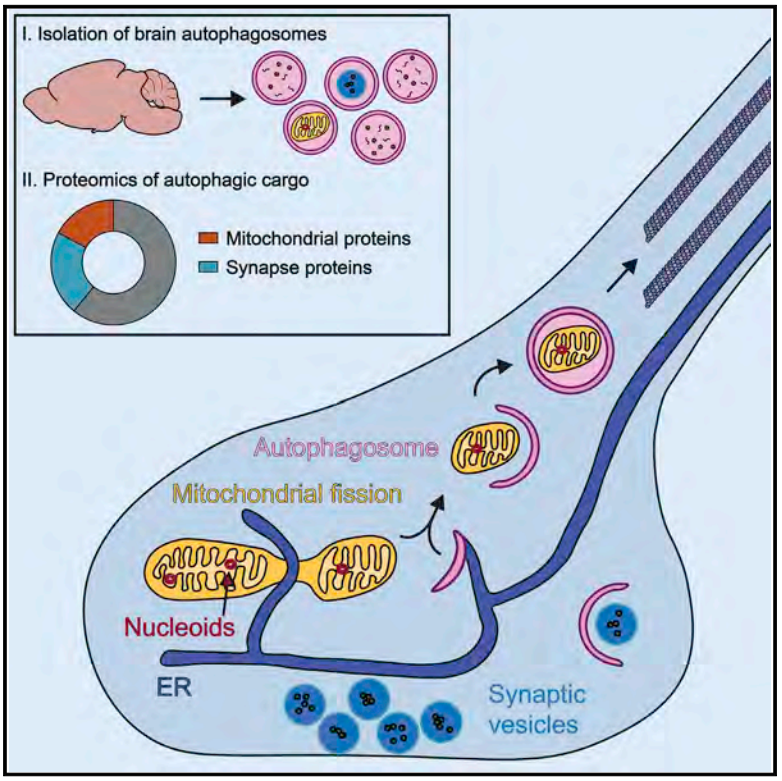

Authors

Juliet Goldsmith, Alban Ordureau, J. Wade Harper, Erika L.F. Holzbaur

Correspondence

holzbaur@pennmedicine.upenn.edu

In brief

Autophagy is a conserved pathway for the degradation of aggregated proteins and dysfunctional organelles that is required for neuronal homeostasis. Goldsmith et al. perform proteomic profiling of cargos degraded by autophagy in brain and neurons under basal conditions, identifying the turnover of mitochondrial nucleoids as a primary function of neuronal autophagy.

Highlights

- Proteomics identify cargos degraded by basal autophagy in brain and neurons
- Synaptic and mitochondrial proteins are predominant cargos for autophagy in neurons
- TFAM-positive mitochondrial nucleoids are enriched in autophagosomes
- Nucleoid-enriched mitochondrial fragments are generated by Drp1-dependent fission

Goldsmith et al., 2022, Neuron *110*, 1–10
March 16, 2022
https://doi.org/10.1016/j.neuron.2021.12.029

CellPress

Neuron

CellPress

Report

Brain-derived autophagosome profiling reveals the engulfment of nucleoid-enriched mitochondrial fragments by basal autophagy in neurons

Juliet Goldsmith,[1] Alban Ordureau,[2,3] J. Wade Harper,[2] and Erika L.F. Holzbaur[1,*]
[1]Department of Physiology, University of Pennsylvania Perelman School of Medicine, Philadelphia, PA 19104, USA
[2]Department of Cell Biology, Blavatnik Institute, Harvard Medical School, Boston, MA 02115, USA
[3]Present address: Cell Biology Program, Sloan Kettering Institute, Memorial Sloan Kettering Cancer Center, New York, NY 10065, USA
*Correspondence: holzbaur@pennmedicine.upenn.edu
https://doi.org/10.1016/j.neuron.2021.12.029

SUMMARY

Neurons depend on autophagy to maintain cellular homeostasis, and defects in autophagy are pathological hallmarks of neurodegenerative disease. To probe the role of basal autophagy in the maintenance of neuronal health, we isolated autophagic vesicles from mouse brain tissue and used proteomics to identify the major cargos engulfed within autophagosomes, validating our findings in rodent primary and human iPSC-derived neurons. Mitochondrial proteins were identified as a major cargo in the absence of mitophagy adaptors such as OPTN. We found that nucleoid-associated proteins are enriched compared with other mitochondrial components. In the axon, autophagic engulfment of nucleoid-enriched mitochondrial fragments requires the mitochondrial fission machinery Drp1. We proposed that localized Drp1-dependent fission of nucleoid-enriched fragments in proximity to the sites of autophagosome biogenesis enhances their capture. The resulting efficient autophagic turnover of nucleoids may prevent accumulation of mitochondrial DNA in the neuron, thus mitigating activation of proinflammatory pathways that contribute to neurodegeneration.

INTRODUCTION

Autophagy is a highly conserved cellular degradation and recycling process that initiates with the formation of a double membrane at the omegasome complex, associated with the endoplasmic reticulum (ER) in mammalian cells. The resulting phagophore elongates through a series of conjugation events that include the insertion of lipidated Atg8-family proteins into the growing membrane of the nascent autophagosome. Cargos destined to be degraded by autophagy are captured by the forming autophagosome either through stochastic bulk engulfment of proteins and small organelles in the vicinity or more selectively via autophagy receptors that deliver specific, often ubiquitylated, cargo to Atg8-family proteins.

A number of studies have begun to define autophagy cargo across model systems. These experiments have used various isolation techniques including differential centrifugation (Dengjel et al., 2012; Mancias et al., 2014; Øverbye et al., 2007), selective pull-downs of Atg8-family proteins (Behrends et al., 2010; Gao et al., 2010; Schmitt et al., 2021), or proximity labeling (Le Guerroué et al., 2017; Zellner et al., 2021). Still to be determined are the cargos degraded by autophagy in neurons under basal conditions. Neurons are postmitotic and long-lived cells and thus are uniquely dependent on the efficient clearance of damaged proteins and dysfunctional organelles via autophagy. Neuron-specific knockout of essential components of the autophagy machinery is sufficient to induce rapid neurodegeneration in mice (Hara et al., 2006; Komatsu et al., 2006). Furthermore, mutations impacting the autophagy pathway contribute to inherited neurodegenerative diseases including ALS/FTD and Parkinson's disease (van Beek et al., 2018), and evidence of impaired autophagy is found in postmortem brain samples from patients with Alzheimer's, Huntington's, and Parkinson's disease (Anglade et al., 1997; Nixon et al., 2005; Tellez-Nagel et al., 1974). The unique dependence of neurons on autophagy to maintain cellular homeostasis is reflected in the spatially specific regulation of the pathway; autophagosomes (APs) form constitutively by synaptic sites in the distal axon, fuse with lysosomes, and are trafficked toward the soma as cargo degradation proceeds (Hill and Colón-Ramos, 2020).

Here, we utilize proteomics to define the proteins captured by basal autophagy in mouse brain. We validate our key findings in primary rodent neurons and human iPSC-derived neurons. We find that both synaptic proteins and mitochondrial fragments are basal cargo in brain- and neuron-derived APs, and we demonstrate a Drp1-dependent mechanism for efficient capture of nucleoid-enriched mitochondrial fragments by locally forming axonal APs. The clearance of nucleoids may be part of an essential homeostatic pathway that balances local energy demands with the mitigation of neuroinflammatory risk posed by accumulation of mitochondrial DNA (mtDNA).

Please cite this article in press as: Goldsmith et al., Brain-derived autophagosome profiling reveals the engulfment of nucleoid-enriched mitochondrial fragments by basal autophagy in neurons, Neuron (2021), https://doi.org/10.1016/j.neuron.2021.12.029

RESULTS AND DISCUSSION

Prior studies have reported the proteins that accumulate following knockout of essential autophagy genes in neurons and other cell types (An et al., 2019, 2020; Kuijpers et al., 2021; Mathew et al., 2014; Zhang et al., 2016). Here, we sought to identify cargos degraded by autophagy in a minimally perturbed system. We used differential centrifugation on discontinuous Nycodenz and Percoll gradients to enrich for autophagic vesicles (AVs) (Figure 1A) (Maday et al., 2012; Strømhaug et al., 1998), which include both newly formed APs and APs that have fused with lysosomes to form autophagolysosomes (APLs). This enrichment protocol avoids selection based on a single marker, thus including mature AVs in which Atg8 family proteins have been externally cleaved by Atg4. Following AV enrichment, we include a Proteinase K digestion step to distinguish between autophagosome cargo destined for degradation and externally associated proteins such as the motors and adaptors that transport AVs retrogradely along the axon (Boecker et al., 2021; Boecker et al., 2021; Cason et al., 2021).

Immunoblots demonstrated that our protocol enriches for AVs marked by lipidated LC3 (LC3-II) (Figures 1B and S1A). Consistent with this enrichment, 70% of vesicles isolated from a GFP-LC3B-expressing transgenic mouse colocalized with GFP (Figure 1C). This represents the lower limit of AV enrichment achieved by fractionation, as not all AVs are expected to incorporate the GFP-LC3B marker. The AV fraction excludes markers of other organelles, including the nucleus, Golgi, ER, and early endosomes (Figures S1B–S1G). Rab7 and Rab11, which mark both late endosomes and AVs, were present in the AV fraction but were degraded by Proteinase K, indicating an association with the external AV membrane (Figures S1C and S1F) (Kuchitsu et al., 2018; Szatmári et al., 2014). Similarly, markers of lysosomes/late endosomes and multivesicular bodies were also degraded by Proteinase K, consistent with evidence that newly formed APs fuse rapidly with lysosomes (Figures S1D, S1G, and S1H) (Maday et al., 2012). Although lysosomal markers were present on the surface of the AVs, most AVs were not acidified, as ~1% of GFP-LC3 AVs enriched from brain were positive for the acidic organelle dye LysoTracker, with an equivalent number identified LysoTracker+;GFP-LC3- (Figure S1I). We examined AV morphology by electron microscopy (EM) and found that >85% of vesicles were clearly delimited by a double membrane, the defining feature of an AP, and ~3% of vesicles were electron dense, suggestive of APLs (Figures S1J and S1K). Combined, these findings indicate 80%–90% of isolated vesicles are bona fide APs, of which 2%–3% are acidified APLs.

Proteomics identify cargos of basal autophagy in the brain

We performed tandem mass tag liquid chromatography mass spectrometry (MS) on the AV and AV + Proteinase K fractions from 7- to 8-month-old mouse brains (Table S1: Proteomic profiling of APs from mouse brain). The ratio of AV+PK/AV, which we call the cargo score, gives an indication of the likelihood that the identified protein is an autophagic cargo destined for degradation. A ranked cargo score plot of brain-derived AVs from five biological replicates displays 4,190 unique proteins (ranked horizontally) with a median cargo score of 0.331 (Figure S2A). We found significant enrichment of two major cargo types: synaptic proteins and mitochondrial proteins. The engulfment and clearance of synaptic and mitochondrial markers by APs in neurons has been previously noted (Hoffmann et al., 2019; Maday et al., 2012), but here, we found that under basal conditions, these cargos are major substrates for autophagy in adult mammalian brain.

Previous studies have identified the autophagic degradation of proteasome components in fibroblasts and cancer cell lines (Dengjel et al., 2012; Schmitt et al., 2021; Zhang et al., 2016); yet, we did not observe an enrichment of proteasome proteins in brain-derived AVs, suggesting cell-type specificity (Figure S2B). A significant accumulation of ER proteins was found in Atg5-deficient neurons (Kuijpers et al., 2021). Although we found calnexin and not calreticulin in our AV fraction consistent with Atg5-deficient neurons (Figure S1B), gene ontology analysis did not identify the ER as one of the top terms (Figures S2C and S2D; (Hung et al., 2017; Moltedo et al., 2019). This may reflect differences between the analysis of basal cargos from adult brain performed here and the analysis of long-term cargo accumulation throughout neuron development, as autophagy plays a role in remodeling the ER early in neuronal differentiation (Ordureau et al., 2021).

To further validate our proteomics dataset, we examined the autophagic engulfment of synaptic proteins, which comprised 16.6% of all proteins identified from the AV-enriched fraction isolated from mouse brain (Figure 1D). We found a significant enrichment of synaptic proteins ($p = 2.93^{-45}$) by gene ontology analysis (Figure 1E) and confirmed that synapsin I, VAMP2, and synaptophysin were present in brain-derived AVs by immunoblotting (Figures 1F[i], S3A, and S3B). Both pre- and post-synaptic proteins were identified (Figures 1E and S3C-S3F), which may reflect engulfment of synaptic proteins in neurons and/or glia within the brain; assessing the relative contributions of neuronal and glial autophagy to synaptic protein turnover will require further investigation Figure S3.

To test whether synapsin is a cargo for autophagy within neurons, we performed a parallel AV enrichment from human iPSC-derived glutamatergic neurons (i^3Neurons; Fernandopulle et al., 2018). Immunoblots indicated that synapsin I is present in both the AV and Proteinase K-protected fractions (Figure 1F[ii]). To verify that synapsin I is present within LC3-positive AVs, we generated an AV fraction from the brains of GFP-LC3 transgenic mice and performed a GFP pulldown to select for LC3-positive AVs only. Immunoblotting of the pulldown fraction showed that synapsin I is an autophagic cargo (Figure 1G). We also performed live imaging in rat primary hippocampal neurons coexpressing GFP-LC3 and mCherry-Synapsin; ~60% of retrogradely trafficking axonal AVs marked by LC3 were positive for synapsin (Figures 1H and S3G). These data are consistent with previous findings on the autophagic turnover of synaptic proteins (Compans et al., 2021; Hoffmann-Conaway et al., 2020; Hoffmann et al., 2019; Nikoletopoulou et al., 2017; Shehata et al., 2012) and further validate our AV enrichment protocol. Although these studies demonstrate a role for basal autophagy in synaptic maintenance, future work is required to determine whether autophagy preferentially turns over "old" synaptic vesicle proteins as predicted (Truckenbrodt et al., 2018).

Please cite this article in press as: Goldsmith et al., Brain-derived autophagosome profiling reveals the engulfment of nucleoid-enriched mitochondrial fragments by basal autophagy in neurons, Neuron (2021), https://doi.org/10.1016/j.neuron.2021.12.029

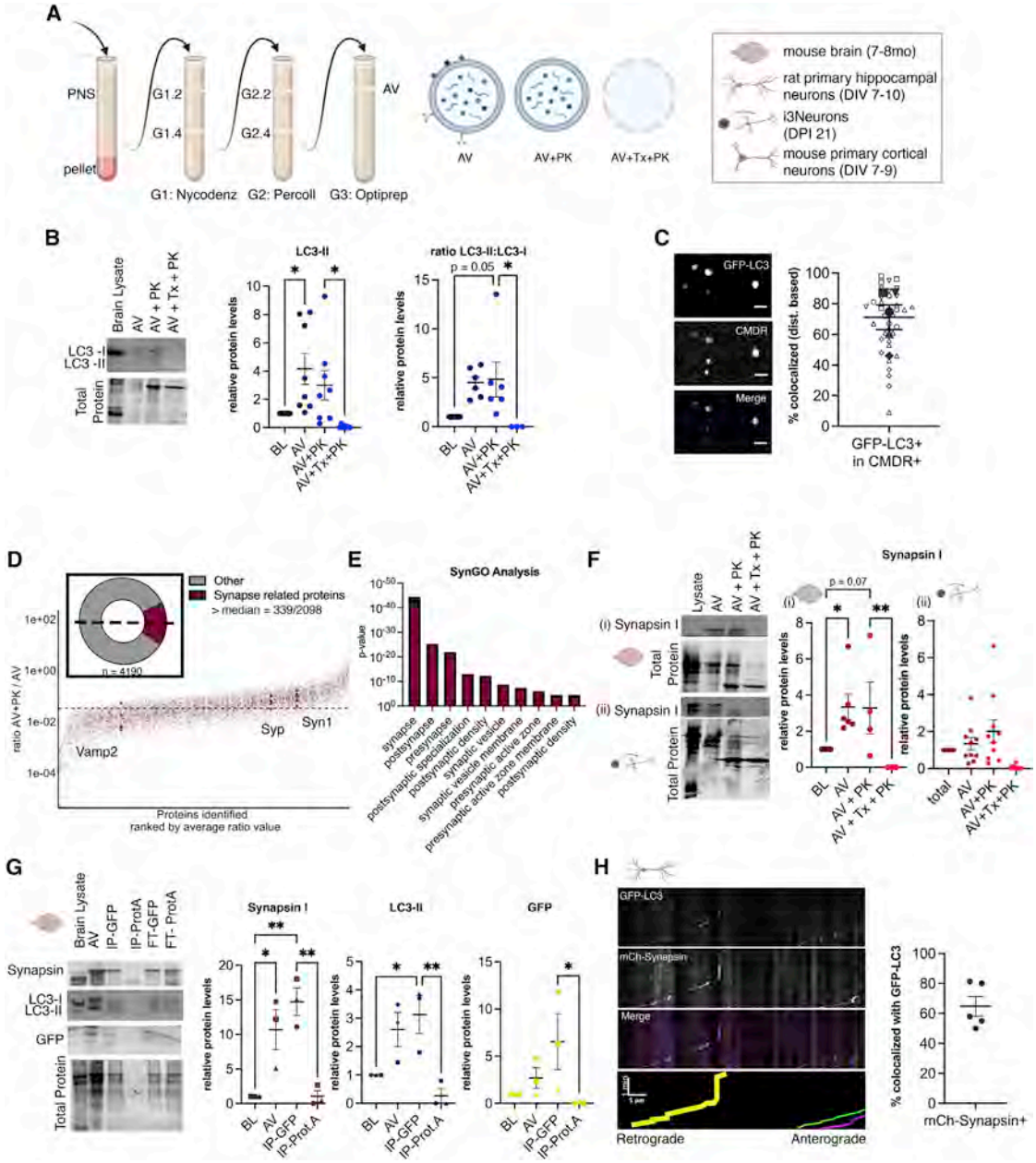

Figure 1. Proteomic profiling of isolated AVs identifies synaptic proteins as an abundant autophagic cargo

(A) Schematic of differential centrifugation protocol to enrich for AVs and AV cargo based on size and density.

(B) Representative immunoblot for LC3 and quantification of the levels of lipidated LC3 (LC3-II) normalized to total protein (n = 11) and the ratio of LC3-II to LC3-I (n = 6) in AV fractions (mean ± SEM, ANOVA with Šídák's, p values: * < 0.05).

(C) AVs from GFP-LC3 transgenic mouse brain were stained with CellMask Deep Red (CMDR) and imaged by spinning disk microscopy (n = 5); percent of GFP-LC3+, CMDR+ puncta was quantified by automated colocalization analysis. Scale bar = 2 μm.

(D) Total fraction (donut plot inset) and ranked cargo score plot of proteomics data, highlighting proteins included in the synapse gene ontology term in maroon. Median cargo score is depicted as dashed lines. Of the proteins that had cargo scores greater than the median value (2,098), 339 (16%) were synapse related.

(E) Graph of p values of the top gene ontology terms from the SynGO database.

(F) Representative immunoblot and quantification of synapsin I levels from (i) brain-derived (n = 6) and (ii) i^{3}Neuron-derived AVs (n = 10) (mean ± SEM, ANOVA with Šídák's, p values: * < 0.05, ** < 0.01).

(G) Representative immunoblot and quantification, normalized to the total protein levels, from GFP-LC3 mouse brain-derived AVs subsequently immunoprecipitated for GFP or Protein A as a negative control (n = 3, ANOVA with Šídák's for TFAM and LC3-II, Kruskal-Wallis with Dunn for GFP, p values: * < 0.05, ** < 0.01). Pulldown (IP) and flow-through (FT) fractions are shown.

(H) Representative kymograph and quantification of trafficking GFP-LC3 puncta that comigrate with mCherry-Synapsin in the mid-axon of primary hippocampal neurons (yellow = Synapsin+, LC3+ trafficking autophagic vesicle; green = LC3+ autophagic vesicle; maroon = Synapsin+ trafficking vesicle; Scale = 5 μm/1 min. Bar: mean ± SEM, n = 5).

Please cite this article in press as: Goldsmith et al., Brain-derived autophagosome profiling reveals the engulfment of nucleoid-enriched mitochondrial fragments by basal autophagy in neurons, Neuron (2021), https://doi.org/10.1016/j.neuron.2021.12.029

Mitochondrial fragments are engulfed by basal autophagy in neurons

Gene ontology analysis found a significant enrichment for mitochondrial proteins ($p = 9.5^{-55}$) as 20% of all identified proteins from our MS analysis are annotated as mitochondrial proteins (Figures 2A and 2B). Immunoblotting confirmed the copurification of mitochondrial proteins, including SOD1, cytochrome-c, and MIRO2 in AVs isolated from mouse brain (Figures S4A, S4B, and S4Ci–xi). Other mitochondrial proteins such as succinate dehydrogenase A (SDHA) were less abundant in the AV fraction, suggesting differential autophagic turnover of mitochondrial proteins in mouse brain, comparable with observations from *Drosophila* (Vincow et al., 2019).

EM analysis confirmed the engulfment of mitochondrial fragments by AVs, as 50% of double membrane vesicles contained cargos with morphologically identifiable mitochondrial-like structure (Figures 2C–2E). The median diameter of mitochondrial fragments engulfed within AVs is 0.59 μm (95% CI = 0.58–0.61), much larger than mitochondrial-derived vesicles (Sugiura et al., 2014). MitoTracker staining of brain-derived GFP-LC3-positive AVs similarly demonstrated ~50% colocalization (Figure 2F) and suggests that mitochondrial fragments within AVs maintain their membrane potential.

Importantly, our data suggest that the mitochondrial fragments are not targeted to APs by PINK1/Parkin-dependent mitophagy. We found no enrichment of either PINK1 or Parkin, nor the selective autophagy receptors optineurin (OPTN), p62/SQSTM1, NDP52, BNIP3L (Nix), or TAX1BP1, by either MS or immunoblotting (Figures 2G–2I, S4Cx–xiv). In contrast, we did note a higher cargo score for the mitophagy and innate-immunity linked protein TBK1 (Figure 2G), recently suggested to associate with mitochondria under homeostatic conditions (Harding et al., 2021). These findings are consistent with PINK1/Parkin-independent autophagic clearance of mitochondria in the absence of induced mitochondrial damage (Le Guerroué et al., 2017; McWilliams et al., 2018; Ordureau et al., 2021).

Mitochondrial nucleoids are enriched in neuronal AVs

To further define which mitochondrial proteins are more likely to be autophagy cargo, we annotated the mitochondrial proteins identified by proteomics based on suborganellar location/function. We found that proteins associated with mitochondrial DNA (mtDNA) had significantly higher cargo scores compared with all mitochondrial proteins or with proteins within the mitochondrial matrix or electron transport chain (Figures 3A, 3B, and S5A).

Mitochondrial transcription factor A (mtTFA/TFAM) is an activator of mitochondrial transcription and a commonly used marker for mitochondrial nucleoids. TFAM is ~4-fold enriched in AVs compared with brain lysate and 2.5-fold enriched over mitochondrial fractionation from brain by immunoblot (Figure 3C). To confirm that TFAM is engulfed within AVs, we performed a GFP pulldown on AVs derived from GFP-LC3 transgenic mouse brains. We found a 5-fold enrichment of TFAM in the GFP pulldown compared with input, indicating that TFAM is present and enriched within LC3-positive AVs (Figure 3D).

To test whether the enrichment of TFAM in AVs occurs in neurons, we immunoblotted AVs isolated from either i^3Neurons or primary mouse cortical neurons and found that TFAM was present in both (Figures 3E and 3F). In contrast, AVs from predifferentiated iPSCs did not have similar levels of TFAM, suggesting that the enrichment of nucleoids within AVs is neuron (and potentially glia) specific (Figure S5B). Consistent with this possibility, meta-analysis showed that nucleoid proteins are not enriched as autophagy cargo in other cell types compared with our findings in brain and neurons (Table S2: Meta-analysis of mtDNA associated proteins identified through autophagosome proteomics, related to Figure 3). One potential explanation is the higher copy number of mtDNA in the brain compared with other tissues (Zhang et al., 2020), resulting in increased basal turnover. A congruent hypothesis is that postmitotic neurons remove extraneous mitochondria via autophagy unlike actively dividing cells.

We found that approximately 50% of all vesicles from the AV fraction were positive for nucleic acids by SYBR staining (Figure 3G). To confirm that the vesicles detected were bona fide AVs, we immunoprecipitated AVs with an anti-LC3 antibody attached to a coverslip, validated the pulldown efficacy (Figure S5C), and stained for nucleic acid with SYBR (Figure S5D), finding consistently that ~50% of the AVs contain nucleic acids. To determine whether this represented mtDNA, we performed qPCR with primers specific for mouse mtDNA (ND2, ND5, and COXII) or nuclear DNA (LINE1) on brain-derived AVs compared with brain lysate. We found that mtDNA was 150-fold enriched over nuclear DNA in AVs (Figure 3H). Thus, we demonstrate that basal neuronal autophagy engulfs mitochondrial fragments containing nucleoids, with no evidence that canonical mitophagy proteins or receptors are involved.

Nucleoid-enriched mitochondrial fragment engulfment by axonal autophagy requires Drp1-dependent mitochondrial fission

To validate the presence of nucleoids within AVs in live neurons, we expressed tagged TFAM and LC3 in primary rat hippocampal neurons for live imaging of AVs traveling retrogradely in the axon. GFP-LC3 and mCherry-LC3 colocalize in the distal and mid axon, therefore we use these markers interchangeably to identify AVs (Figure S6A). 10%–20% of AVs identified by tagged LC3 were positive for either mito-dsRed or Cox8a, respectively, consistent with previous reports (Maday et al., 2012; Wong and Holzbaur, 2014). In contrast, 40% of trafficking AVs were positive for TFAM (Figures 4A–4C, and S6B). Thus, autophagic engulfment of nucleoid-enriched mitochondrial fragments occurs under basal conditions in the axon.

EM suggested that the contents of APs can be heterogenous (Figure 2C), so we investigated whether two validated AV cargos from neurons, TFAM and synapsin, are individually engulfed by APs or capable of cocapture, suggestive of bulk engulfment. Consistent with nonselective uptake, we found that about half of synapsin-positive trafficking AVs were also positive for TFAM (Figures 4D–4F).

Mitochondrial dynamics via fission and fusion are essential for their function. Drp1-dependent fission has been shown to occur at the mitochondria–ER contact sites, which also define the sites of mtDNA replication (Friedman et al., 2011; Lewis et al., 2016). We investigated whether mitochondrial fission machinery was required for basal autophagic capture of nucleoid-enriched mitochondrial fragments. Overexpression of dominant negative

Please cite this article in press as: Goldsmith et al., Brain-derived autophagosome profiling reveals the engulfment of nucleoid-enriched mitochondrial fragments by basal autophagy in neurons, Neuron (2021), https://doi.org/10.1016/j.neuron.2021.12.029

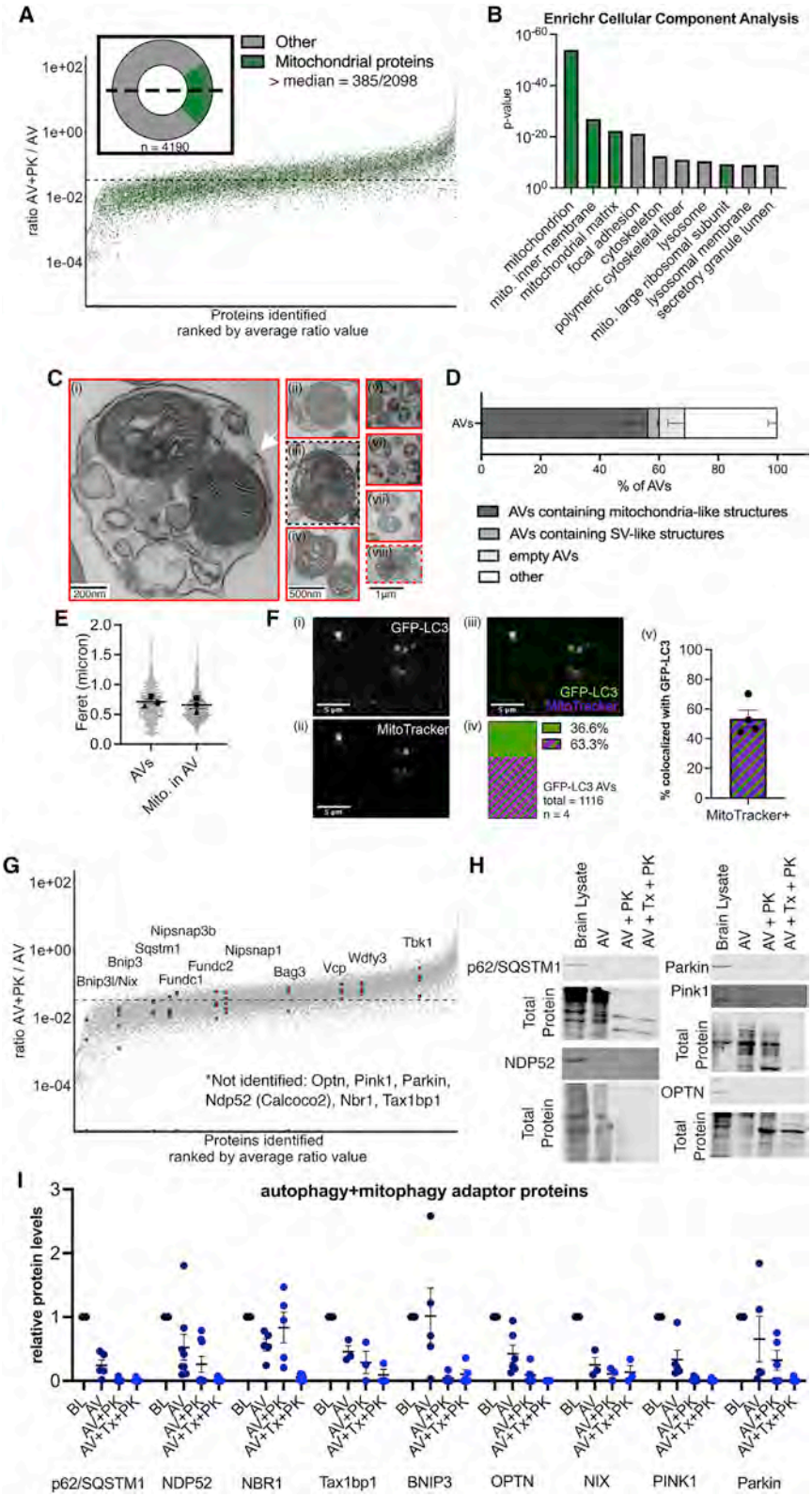

Figure 2. Basal brain-derived autophagic vesicles are enriched for mitochondrial fragments, not autophagy adaptors or mitophagy proteins

(A) Total fraction (donut plot inset) and ranked cargo score plot of proteomics data highlighting mitochondrial proteins in green. Median cargo score is depicted as dashed lines. Of the proteins that had cargo scores greater than the median value (2,098), 385 (18%) were mitochondrial.

(B) Graph of p values of the top gene ontology terms for cellular component from the Enrichr database.

(C) Representative electron micrographs. Indicated are the double membrane (arrow), AVs with mitochondria-like cargo (red boxes; i–ii, iv–viii), AVs with synaptic vesicle-like cargo (dashed boxes; iii, viii), and AVs with heterogeneous cargo (i–iii, vii–viii). Scale bars: (i) = 200 nm; (ii)-(iv) = 500 nm; (v)-(viii) = 1 μm.

(D) Quantification of types of AV cargo from EM (n = 3, total events = 1,409).

(E) Quantification of diameter of AVs and mitochondrial cargo by EM (n = 3, total events ≥ 1,262).

(F) AVs enriched from GFP-LC3 transgenic mouse brain homogenate were stained using MitoTracker Deep Red and imaged by spinning disk microscopy (n = 4); (i–iii) representative image, percent of GFP-LC3+, MitoTracker+ puncta was quantified over and (iv) all events counted and (v) biological replicates. Scale bar = 5 μm.

(G) Ranked cargo score plot, highlighting autophagy adaptors and assoicated proteins in red.

(H and I) Select representative images and quantification of immunoblotting, normalized to total protein levels, for autophagy receptors and mitophagy-related proteins in brain-derived AVs (n ≥ 3). See Figure S4 (x–xiv) for additional representative immunoblots.

Please cite this article in press as: Goldsmith et al., Brain-derived autophagosome profiling reveals the engulfment of nucleoid-enriched mitochondrial fragments by basal autophagy in neurons, Neuron (2021), https://doi.org/10.1016/j.neuron.2021.12.029

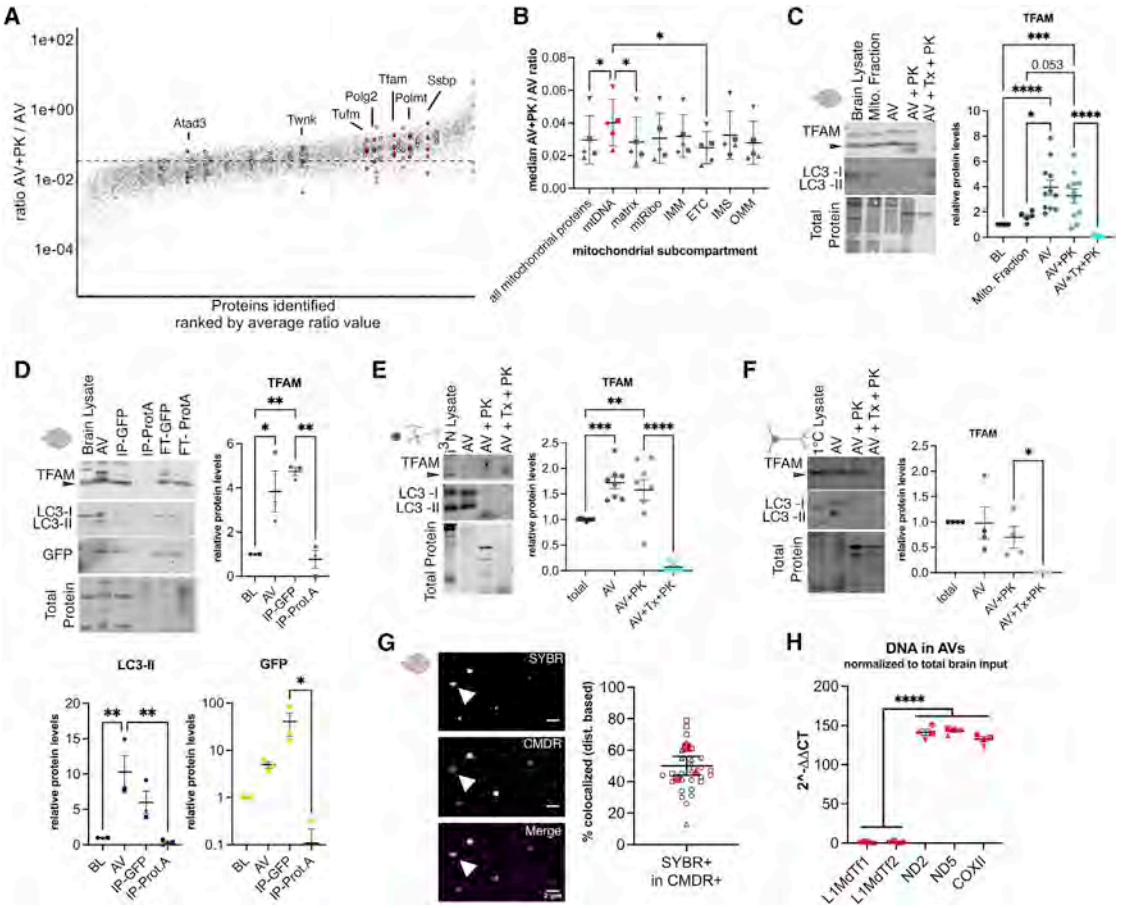

Figure 3. Nucleoid-enriched mitochondrial fragments containing TFAM and mtDNA are cargo in brain-derived and neuron-derived autophagic vesicles

(A) Ranked cargo score plot, highlighting well-characterized mitochondrial nucleoid proteins (red) and nucleoid-associated proteins (pink) (He et al., 2012).

(B) Plot of median cargo scores across different subgroups of mitochondrial proteins (mean ± SEM, n = 5, ANOVA with Dunnett's, p value: * < 0.05). See Figure S5A for violin plot of individual protein values.

(C) Representative immunoblot and quantification of levels of TFAM, normalized to total protein, from brain-derived input, crude mitochondrial preparations, and AV fractions (n ≥ 5; ANOVA with Šídák's, p values: * < 0.05, *** < 0.001, **** < 0.0001).

(D) Representative immunoblot and quantification, normalized to total protein levels, from GFP-LC3 mouse brain-derived AVs subsequently immunoprecipitated with anti-GFP antibody, Protein A was the negative control (n = 3, ANOVA with Šídák's for TFAM and LC3-II, Kruskal-Wallis with Dunn for GFP, p values: * < 0.05, ** < 0.01). Pulldown (IP) and flow-through (FT) fractions are shown.

(E and F) Representative immunoblot and quantification of levels of TFAM, normalized to total protein levels, from AV fractions from (E) i^{3}Neurons (n = 8) and (F) primary cortical neurons (n = 4), (ANOVA with Šídák's, p values: * < 0.05, ** < 0.01, *** < 0.001, **** < 0.0001).

(G) Representative confocal microscopy images and quantification of AVs enriched from brain homogenate stained for membrane (CMDR) or nucleic acids (SYBR gold) (n = 3). Scale bar = 2 μm.

(H) qPCR for nuclear DNA (LINE sequences L1MdTf1 and L1MdTf2) and mitochondrial DNA (ND2, ND5, and COXII) was performed on DNA extracted from brain-derived AVs. The relative fold change ($2^{\Delta\Delta CT}$) is plotted (mean ± SEM, n = 4, ANOVA with Dunnett's).

Drp1 (GFP-Drp1^{K38A}) abrogated the levels of TFAM within AVs (Figures 4G–4I). Drp1 is necessary but not sufficient for AV engulfment of nucleoid-enriched mitochondrial fragments, as overexpression of wildtype Drp1 did not lead to increased levels of TFAM in trafficking AVs (Figure 4H). Fission factors that distinguish the fate of the mitochondrial fragments have recently been described in Cos7 cells (Kleele et al., 2021): products of ER-associated, Mff-dependent fission commonly contain mtDNA and contribute to mitochondrial biogenesis, whereas products of lysosome-associated, Fis1-dependent fission commonly contain markers of mitochondrial damage and are degraded via mitophagy. Immunoblotting analysis indicates that Mff—but not Drp1, Fis1, or mitochondrial fusion proteins—is present in our AV fractions (Figures 4J, S6C, and S6D), suggesting that axonal APs engulf nucleoid-containing mitochondrial fragments generated through normal, rather than damage-associated, fission processes.

What is driving nucleoid-enriched mitochondrial fragments to APs in the absence of autophagy receptors? We postulate that in neurons, Drp1- and Mff-dependent mitochondrial fission occurs at mitochondria–ER contact sites, which ensures that nucleoid-enriched mitochondrial fragments are generated in close

Please cite this article in press as: Goldsmith et al., Brain-derived autophagosome profiling reveals the engulfment of nucleoid-enriched mitochondrial fragments by basal autophagy in neurons, Neuron (2021), https://doi.org/10.1016/j.neuron.2021.12.029

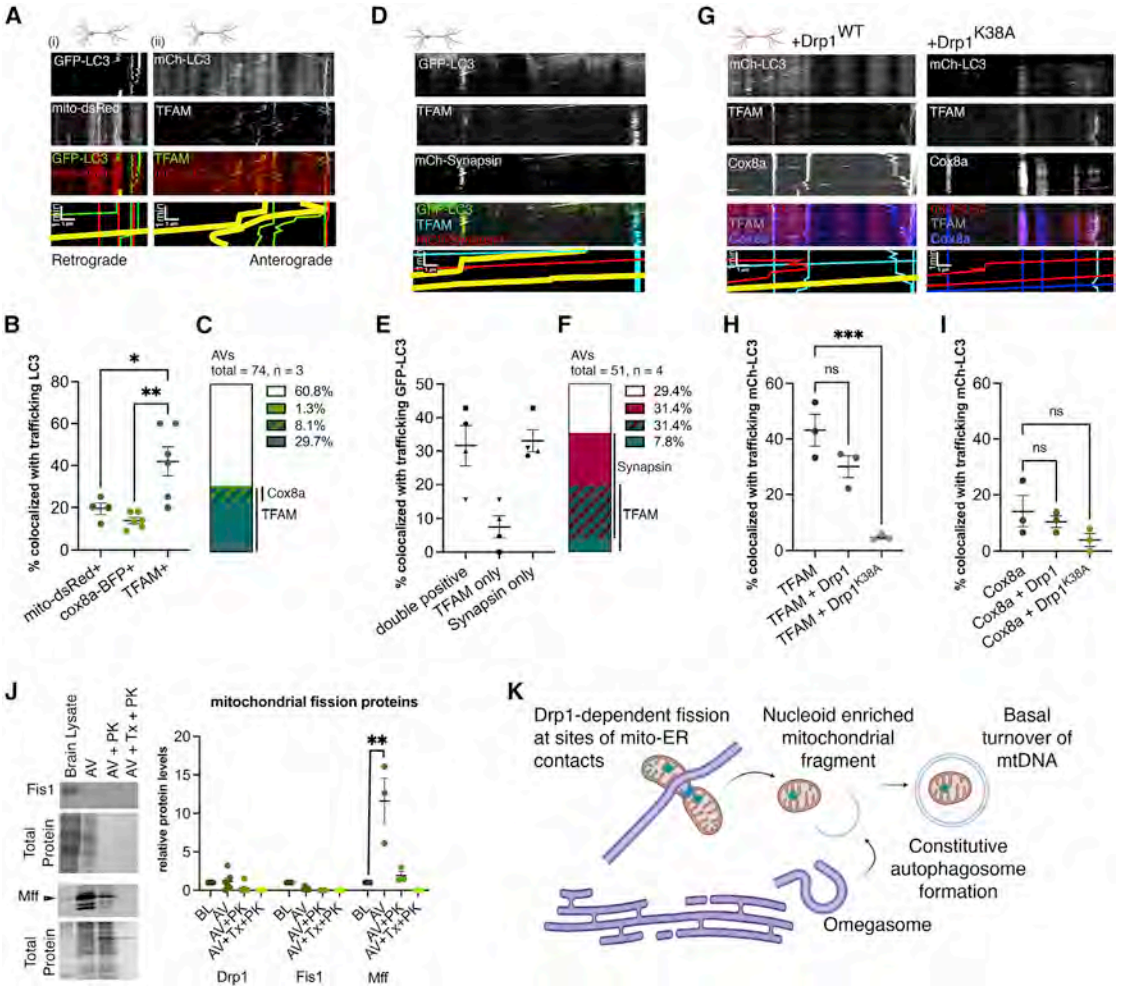

Figure 4. Drp1 is required for nucleoid-enriched mitochondrial fragment engulfment by autophagosomes in neurons

(A–C) (A) Representative kymographs and (B and C) quantification from primary hippocampal neurons expressing markers of mitochondria (mito-dsRed and Cox8a-BFP) or Snap-TFAM and fluorescently tagged LC3 (as indicated) as a marker for AVs. (Ai: yellow = mito-dsRed+, LC3+ trafficking AV; green = LC3+ AV; red = mito-dsRed+ vesicle; Aii: yellow = TFAM+, LC3+ trafficking AV; green = TFAM+ vesicle; red = LC3+ AV; Scale = 5 μm/1 min) (Bar: mean ± SEM, n ≥ 4, ANOVA with Šídák's, p values: * < 0.05, ** < 0.01).

(D–F) (D) Representative kymograph and (E and F) quantification from primary hippocampal neurons expressing GFP-LC3 to identify AVs, Snap-TFAM and mCherry-Synapsin to identify cotrafficking of AV cargo. (D: yellow = TFAM+, synapsin+, LC3+ trafficking AV; red= synapsin+, LC3+ trafficking AV; cyan = TFAM+ vesicle; Scale = 5 μm/1 min) (Bar: mean ± SEM, n = 4 ANOVA with Šídák's).

(G–I) (G) Representative kymograph and (H and I) quantification from primary hippocampal neurons expressing GFP-tagged wild-type Drp1 or dominant negative $Drp1^{K38A}$ with Snap-TFAM, Cox8a-BFP, and mCherry-LC3. (G: yellow = TFAM+, LC3+ trafficking AV; red = LC3+ AV; cyan = Cox8a+, TFAM+ vesicle; blue = Cox8a+ vesicle; Scale = 5 μm/1 min) (Bar: mean ± SEM, n = 3, ANOVA with Šídák's, p values: ns = not significant, *** < 0.001).

(J) Representative immunoblot and quantification of levels of mitochondrial fission machinery, normalized to total protein, from brain-derived AVs (Bar: mean ± SEM, n ≥ 3, ANOVA with Šídák's, p value: ** < 0.01). Additional representative immunoblot in Figure S6C.

(K) Model of engulfment of nucleoid-enriched mitochondrial fragments by forming APs in neurons.

proximity to phagophore formation from the ER-associated omegasomes. Thus, newly forming APs are optimally localized to sweep up nucleoid-enriched mitochondrial fragments through bulk engulfment without necessitating adaptor proteins (Figure 4K). Whether this pathway contributes to maintaining mitochondrial genome integrity, as recently ascribed to PINK1/Parkin mitophagy (Ahier et al., 2021), remains to be determined. This model predicts that disruption of basal autophagy, either by aging (Stavoe et al., 2019) or neurodegenerative disease mutations, would result in mtDNA accumulation that may sensitize neurons to proinflammatory signaling (Borsche et al., 2020). As mutant TDP-43 and Huntingtin were recently demonstrated to induce release of mtDNA and mtRNA, respectively, resulting in inflammation (Lee et al., 2020; Yu et al., 2020), further deficits in autophagy with age could exacerbate pathogenic inflammation in neurodegenerative disease by increasing mtDNA levels.

We speculate that basal autophagy maintains homeostatic balance in the neuron, in great part due to the nonselective nature of turnover. Since both mitochondria and synapse proteins were identified as key cargo, basal autophagy may balance

energy production with the demands of synaptic transmission. Our evidence strongly suggests autophagic engulfment of nucleoid-enriched mitochondrial fragments is a distinct pathway from the targeted removal of damaged mitochondria; therefore, a balance between the two processes could maintain a healthy mitochondrial population locally and temporally. Finally, basal autophagy may balance the high energy requirements of neurons with the increased inflammation risk caused by accumulation of mtDNA.

STAR★METHODS

Detailed methods are provided in the online version of this paper and include the following:

- KEY RESOURCES TABLE
- RESOURCE AVAILABILITY
  - Lead contact
  - Materials availability
  - Data and code availability
- EXPERIMENTAL MODEL AND SUBJECT DETAILS
  - Animal models
  - Cell lines, primary cultures
- METHOD DETAILS
  - Isolation of autophagic vesicles by differential centrifugation
  - Crude mitochondrial fraction enrichment
  - Proteomics—sample preparation and digestion
  - Proteomics—Off-line basic pH reversed-phase (BPRP) fractionation
  - Proteomics—Liquid chromatography and tandem mass spectrometry
  - Proteomics—Data analysis
  - Immunoblotting
  - GFP immunoprecipitation
  - Transfection for live imaging
  - Electron microscopy
  - Immunofluorescence of AVs
  - qPCR
- QUANTIFICATION AND STATISTICAL ANALYSIS

SUPPLEMENTAL INFORMATION

Supplemental information can be found online at https://doi.org/10.1016/j.neuron.2021.12.029.

ACKNOWLEDGMENTS

We thank Adam R. Fenton for graphical abstract design, Mariko Tokito for assistance in the cloning of plasmid constructs, Karen Wallace Jahn for assistance with animal models, and J.A. Paulo for proteomics support. This research was supported by the National Institutes of Health grants NS060698 (E.L.F.H.), NS083524 (J.W.H.), and NS110395 (J.W.H.).

AUTHOR CONTRIBUTIONS

J.G., E.L.F.H., and J.W.H., project design and conceptualization; J.G. and E.L.F.H., co-writing – original draft; J.G., E.L.F.H., J.W.H., and A.O., editing the manuscript; A.O., proteomics data collection and analysis; J.G., resources, data collection, data analysis, and interpretation; and E.L.F.H. and J.W.H., funding acquisition.

DECLARATION OF INTERESTS

J.W.H. is a consultant and founder of Caraway Therapeutics and is a founding board member of Interline Therapeutics. J.W.H. also receives compensation for editorial service at eLife and Science Advances. E.H. receives compensation for editorial service from Science Advances.

INCLUSION AND DIVERSITY

We worked to ensure sex balance in the selection of non-human subjects. While citing references scientifically relevant for this work, we also actively worked to promote gender balance in our reference list.

Received: June 17, 2021
Revised: October 18, 2021
Accepted: December 16, 2021
Published: January 19, 2022

REFERENCES

Ahier, A., Dai, C.-Y., Kirmes, I., Cummins, N., Hung, G.C.C., Götz, J., and Zuryn, S. (2021). PINK1 and parkin shape the organism-wide distribution of a deleterious mitochondrial genome. Cell Rep *35*, 109203. https://doi.org/10.1016/j.celrep.2021.109203.

An, H., Ordureau, A., Körner, M., Paulo, J.A., and Harper, J.W. (2020). Systematic quantitative analysis of ribosome inventory during nutrient stress. Nature *583*, 303–309. https://doi.org/10.1038/s41586-020-2446-y.

An, H., Ordureau, A., Paulo, J.A., Shoemaker, C.J., Denic, V., and Harper, J.W. (2019). TEX264 is an endoplasmic reticulum-resident ATG8-interacting protein critical for ER remodeling during nutrient stress. Mol. Cell *74*, 891–908.e10. https://doi.org/10.1016/j.molcel.2019.03.034.

Anglade, P., Vyas, S., Javoy-Agid, F., Herrero, M.T., Michel, P.P., Marquez, J., Mouatt-Prigent, A., Ruberg, M., Hirsch, E.C., and Agid, Y. (1997). Apoptosis and autophagy in nigral neurons of patients with Parkinson's disease. Histol. Histopathol. *12*, 25–31.

Behrends, C., Sowa, M.E., Gygi, S.P., and Harper, J.W. (2010). Network organization of the human autophagy system. Nature *466*, 68–76. https://doi.org/10.1038/nature09204.

Boecker, C.A., Olenick, M.A., Gallagher, E.R., Ward, M.E., and Holzbaur, E.L.F. (2019). ToolBox: Live Imaging of intracellular organelle transport in induced pluripotent stem cell-derived neurons. Traffic *September 2019*, 138–155. https://doi.org/10.1111/tra.12701.

Boecker, C.A., Goldsmith, J., Dou, D., Cajka, G.G., and Holzbaur, E.L.F. (2021). Increased LRRK2 kinase activity alters neuronal autophagy by disrupting the axonal transport of autophagosomes. Curr. Biol. *31*, 2140–2154.e6. https://doi.org/10.1016/j.cub.2021.02.061.

Borsche, M., König, I.R., Delcambre, S., Petrucci, S., Balck, A., Brüggemann, N., Zimprich, A., Wasner, K., Pereira, S.L., Avenali, M., et al. (2020). Mitochondrial damage-associated inflammation highlights biomarkers in PRKN/PINK1 parkinsonism. Brain *143*, 3041–3051. https://doi.org/10.1093/brain/awaa246.

Calvo, S.E., Clauser, K.R., and Mootha, V.K. (2016). MitoCarta2.0: an updated inventory of mammalian mitochondrial proteins. Nucleic Acids Res *44*, D1251–D1257. https://doi.org/10.1093/nar/gkv1003.

Cason, S.E., Carman, P.J., Van Duyne, C., Goldsmith, J., Dominguez, R., and Holzbaur, E.L.F. (2021). Sequential dynein effectors regulate axonal autophagosome motility in a maturation-dependent pathway. J. Cell Biol. *220*. https://doi.org/10.1083/jcb.202010179.

Chen, E.Y., Tan, C.M., Kou, Y., Duan, Q., Wang, Z., Meirelles, G.V., Clark, N.R., and Ma'ayan, A. (2013). Enrichr: interactive and collaborative HTML5 gene list enrichment analysis tool. BMC Bioinformatics *14*, 128. https://doi.org/10.1186/1471-2105-14-128.

Compans, B., Camus, C., Kallergi, E., Sposini, S., Martineau, M., Butler, C., Kechkar, A., Klaassen, R.V., Retailleau, N., Sejnowski, T.J., et al. (2021). NMDAR-dependent long-term depression is associated with increased short

term plasticity through autophagy mediated loss of PSD-95. Nat. Commun. *12*, 2849. https://doi.org/10.1038/s41467-021-23133-9.

Dengjel, J., Høyer-Hansen, M., Nielsen, M.O., Eisenberg, T., Harder, L.M., Schandorff, S., Farkas, T., Kirkegaard, T., Becker, A.C., Schroeder, S., et al. (2012). Identification of autophagosome-associated proteins and regulators by quantitative proteomic analysis and genetic screens. Mol. Cell. Proteomics *11*. M111.014035. https://doi.org/10.1074/mcp.M111.014035.

Eng, J.K., Jahan, T.A., and Hoopmann, M.R. (2013). Comet: an open-source MS/MS sequence database search tool. Proteomics *13*, 22–24. https://doi.org/10.1002/pmic.201200439.

Erickson, B.K., Mintseris, J., Schweppe, D.K., Navarrete-Perea, J., Erickson, A.R., Nusinow, D.P., Paulo, J.A., and Gygi, S.P. (2019). Active instrument engagement combined with a real-time database search for improved performance of sample multiplexing workflows. J. Proteome Res. *18*, 1299–1306. https://doi.org/10.1021/acs.jproteome.8b00899.

Fernandopulle, M.S., Prestil, R., Grunseich, C., Wang, C., Gan, L., and Ward, M.E. (2018). Transcription factor mediated-differentiation of human iPSCs into neurons. Curr. Protoc. Cell Biol. *79*, e51. https://doi.org/10.1002/cpcb.51.

Friedman, J.R., Lackner, L.L., West, M., DiBenedetto, J.R., Nunnari, J., and Voeltz, G.K. (2011). ER tubules mark sites of mitochondrial division. Science *334*, 358–362. https://doi.org/10.1126/science.1207385.

Gao, W., Kang, J.H., Liao, Y., Ding, W.-X., Gambotto, A.A., Watkins, S.C., Liu, Y.-J., Stolz, D.B., and Yin, X.-M. (2010). Biochemical isolation and characterization of the tubulovesicular LC3-positive autophagosomal compartment. J. Biol. Chem. *285*, 1371–1383. https://doi.org/10.1074/jbc.M109.054197.

Hara, T., Nakamura, K., Matsui, M., Yamamoto, A., Nakahara, Y., Suzuki-Migishima, R., Yokoyama, M., Mishima, K., Saito, I., Okano, H., and Mizushima, N. (2006). Suppression of basal autophagy in neural cells causes neurodegenerative disease in mice. Nature *441*, 885–889. https://doi.org/10.1038/nature04724.

Harding, O., Evans, C.S., Ye, J., Cheung, J., Maniatis, T., and Holzbaur, E.L.F. (2021). ALS- and FTD-associated missense mutations in TBK1 differentially disrupt mitophagy. Proc. Natl. Acad. Sci. USA *118*, e2025053118.

He, J., Cooper, H.M., Reyes, A., Di Re, M., Sembongi, H., Litwin, T.R., Gao, J., Neuman, K.C., Fearnley, I.M., Spinazzola, A., et al. (2012). Mitochondrial nucleoid interacting proteins support mitochondrial protein synthesis. Nucleic Acids Res *40*, 6109–6121. https://doi.org/10.1093/nar/gks266.

Hill, S.E., and Colón-Ramos, D.A. (2020). The journey of the synaptic autophagosome: a cell biological perspective. Neuron *105*, 961–973. https://doi.org/10.1016/j.neuron.2020.01.018.

Hoffmann, S., Orlando, M., Andrzejak, E., Bruns, C., Trimbuch, T., Rosenmund, C., Garner, C.C., and Ackermann, F. (2019). Light-activated ROS production induces synaptic autophagy. J. Neurosci. *39*, 2163–2183. https://doi.org/10.1523/JNEUROSCI.1317-18.2019.

Hoffmann-Conaway, S., Brockmann, M.M., Schneider, K., Annamneedi, A., Rahman, K.A., Bruns, C., Textoris-Taube, K., Trimbuch, T., Smalla, K.-H., Rosenmund, C., et al. (2020). Parkin contributes to synaptic vesicle autophagy in bassoon-deficient mice. Elife *9*, e56590. https://doi.org/10.7554/eLife.56590.

Hung, V., Lam, S.S., Udeshi, N.D., Svinkina, T., Guzman, G., Mootha, V.K., Carr, S.A., and Ting, A.Y. (2017). Proteomic mapping of cytosol-facing outer mitochondrial and ER membranes in living human cells by proximity biotinylation. Elife *6*, e24463. https://doi.org/10.7554/eLife.24463.

Huttlin, E.L., Jedrychowski, M.P., Elias, J.E., Goswami, T., Rad, R., Beausoleil, S.A., Villén, J., Haas, W., Sowa, M.E., and Gygi, S.P. (2010). A tissue-specific atlas of mouse protein phosphorylation and expression. Cell *143*, 1174–1189. https://doi.org/10.1016/j.cell.2010.12.001.

Kabeya, Y., Mizushima, N., Ueno, T., Yamamoto, A., Kirisako, T., Noda, T., Kominami, E., Ohsumi, Y., and Yoshimori, T. (2000). LC3, a mammalian homolog of yeast Apg8p, is localized in autophagosome membranes after processing. EMBO Journal *19*, 5720–5728. https://doi.org/10.1093/emboj/cdg454.

Kleele, T., Rey, T., Winter, J., Zaganelli, S., Mahecic, D., Perreten Lambert, H., Ruberto, F.P., Nemir, M., Wai, T., Pedrazzini, T., and Manley, S. (2021). Distinct fission signatures predict mitochondrial degradation or biogenesis. Nature *593*, 435–439. https://doi.org/10.1038/s41586-021-03510-6.

Komatsu, M., Waguri, S., Chiba, T., Murata, S., Iwata, J.-i., Tanida, I., Ueno, T., Koike, M., Uchiyama, Y., Kominami, E., and Tanaka, K. (2006). Loss of autophagy in the central nervous system causes neurodegeneration in mice. Nature *441*, 880–884. https://doi.org/10.1038/nature04723.

Koopmans, F., van Nierop, P., Andres-Alonso, M., Byrnes, A., Cijsouw, T., Coba, M.P., Cornelisse, L.N., Farrell, R.J., Goldschmidt, H.L., Howrigan, D.P., et al. (2019). Syngo: an evidence-based, expert-curated knowledge base for the synapse. Neuron *103*, 217–234.e4. https://doi.org/10.1016/j.neuron.2019.05.002.

Kuchitsu, Y., Homma, Y., Fujita, N., and Fukuda, M. (2018). Rab7 knockout unveils regulated autolysosome maturation induced by glutamine starvation. J. Cell Sci. *131*. https://doi.org/10.1242/jcs.215442.

Kuijpers, M., Kochlamazashvili, G., Stumpf, A., Puchkov, D., Swaminathan, A., Lucht, M.T., Krause, E., Maritzen, T., Schmitz, D., and Haucke, V. (2021). Neuronal autophagy regulates presynaptic neurotransmission by controlling the axonal endoplasmic reticulum. Neuron *109*, 299–313.e9. https://doi.org/10.1016/j.neuron.2020.10.005.

Kuleshov, M.V., Jones, M.R., Rouillard, A.D., Fernandez, N.F., Duan, Q., Wang, Z., Koplev, S., Jenkins, S.L., Jagodnik, K.M., Lachmann, A., et al. (2016). Enrichr: a comprehensive gene set enrichment analysis web server 2016 update. Nucleic Acids Res *44*, W90–W97. https://doi.org/10.1093/nar/gkw377.

Le Guerroué, F., Eck, F., Jung, J., Starzetz, T., Mittelbronn, M., Kaulich, M., and Behrends, C. (2017). Autophagosomal content profiling reveals an LC3C-dependent piecemeal mitophagy pathway. Mol. Cell *68*, 786–796.e6. https://doi.org/10.1016/j.molcel.2017.10.029.

Lee, H., Fenster, R.J., Pineda, S.S., Gibbs, W.S., Mohammadi, S., Davila-Velderrain, J., Garcia, F.J., Therrien, M., Novis, H.S., Gao, F., et al. (2020). Cell type-specific transcriptomics reveals that mutant huntingtin leads to mitochondrial RNA release and neuronal innate immune activation. Neuron *107*, 891–908.e8. https://doi.org/10.1016/j.neuron.2020.06.021.

Lewis, S.C., Uchiyama, L.F., and Nunnari, J. (2016). ER-mitochondria contacts couple mtDNA synthesis with mitochondrial division in human cells. Science *353*, aaf5549. https://doi.org/10.1126/science.aaf5549.

Maday, S., and Holzbaur, E.L.F. (2014). Autophagosome biogenesis in primary neurons follows an ordered and spatially regulated pathway. Dev. Cell *30*, 71–85. https://doi.org/10.1016/j.devcel.2014.06.001.

Maday, S., Wallace, K.E., and Holzbaur, E.L.F. (2012). Autophagosomes initiate distally and mature during transport toward the cell soma in primary neurons. J. Cell Biol. *196*, 407–417. https://doi.org/10.1083/jcb.201106120.

Mancias, J.D., Wang, X., Gygi, S.P., Harper, J.W., and Kimmelman, A.C. (2014). Quantitative proteomics identifies NCOA4 as the cargo receptor mediating ferritinophagy. Nature *509*, 105–109. https://doi.org/10.1038/nature13148.

Mathew, R., Khor, S., Hackett, S.R., Rabinowitz, J.D., Perlman, D.H., and White, E. (2014). Functional role of autophagy-mediated proteome remodeling in cell survival signaling and innate immunity. Mol. Cell *55*, 916–930. https://doi.org/10.1016/j.molcel.2014.07.019.

McAlister, G.C., Nusinow, D.P., Jedrychowski, M.P., Wühr, M., Huttlin, E.L., Erickson, B.K., Rad, R., Haas, W., and Gygi, S.P. (2014). MultiNotch MS3 enables accurate, sensitive, and multiplexed detection of differential expression across cancer cell line proteomes. Anal. Chem. *86*, 7150–7158. https://doi.org/10.1021/ac502040v.

McWilliams, T.G., Prescott, A.R., Montava-Garriga, L., Ball, G., Singh, F., Barini, E., Muqit, M.M.K., Brooks, S.P., and Ganley, I.G. (2018). Basal mitophagy occurs independently of PINK1 in mouse tissues of high metabolic demand. Cell Metab *27*, 439–449.e5. https://doi.org/10.1016/j.cmet.2017.12.008.

Mizushima, N., Yamamoto, A., Matsui, M., Yoshimori, T., and Ohsumi, Y. (2004). In vivo analysis of autophagy in response to nutrient starvation using transgenic mice expressing a fluorescent autophagosomes marker.

Molecular Biology of the Cell *15*, 1101–1111. https://doi.org/10.1091/mbc.E03–09–0704.

Moltedo, O., Remondelli, P., and Amodio, G. (2019). The mitochondria–endoplasmic reticulum contacts and their critical role in aging and age-associated diseases. Front. Cell Dev. Biol. *7*, 172. https://doi.org/10.3389/fcell.2019.00172.

Nikoletopoulou, V., Sidiropoulou, K., Kallergi, E., Dalezios, Y., and Tavernarakis, N. (2017). Modulation of autophagy by BDNF underlies synaptic plasticity. Cell Metab *26*, 230–242.e5. https://doi.org/10.1016/j.cmet.2017.06.005.

Nixon, R.A., Wegiel, J., Kumar, A., Yu, W.H., Peterhoff, C., Cataldo, A., and Cuervo, A.M. (2005). Extensive involvement of autophagy in Alzheimer's disease: an immuno-electron microscopy study. J. Neuropathol. Exp. Neurol. *64*, 113–122.

Ordureau, A., Kraus, F., Zhang, J., An, H., Park, S., Ahfeldt, T., Paulo, J.A., and Harper, J.W. (2021). Temporal proteomics during neurogenesis reveals large-scale proteome and organelle remodeling via selective autophagy. Mol. Cell *81*, 5082–5098.e11. https://doi.org/10.1016/j.molcel.2021.10.001.

Øverbye, A., Fengsrud, M., and Seglen, P.O. (2007). Proteomic analysis of membrane-associated proteins from rat liver autophagosomes. Autophagy *3*, 300–322. https://doi.org/10.4161/auto.3910.

Paulo, J.A., O'Connell, J.D., and Gygi, S.P. (2016). A triple knockout (TKO) proteomics standard for diagnosing ion interference in isobaric labeling experiments. J. Am. Soc. Mass Spectrom. *27*, 1620–1625. https://doi.org/10.1007/s13361-016-1434-9.

Rad, R., Li, J., Mintseris, J., O'Connell, J., Gygi, S.P., and Schweppe, D.K. (2021). Improved monoisotopic mass estimation for deeper proteome coverage. J. Proteome Res. *20*, 591–598. https://doi.org/10.1021/acs.jproteome.0c00563.

Savitski, M.M., Wilhelm, M., Hahne, H., Kuster, B., and Bantscheff, M. (2015). A scalable approach for protein false discovery rate estimation in large proteomic data sets. Mol. Cell. Proteomics *14*, 2394–2404. https://doi.org/10.1074/mcp.M114.046995.

Schmitt, D., Bozkurt, S., Henning-Domres, P., and Kern, A. (2021). Protein content and lipid profiling of isolated native autophagosomes. bioRxiv http://biorxiv.org/cgi/content/short/2021.04.16.440117v1?rss=1&utm_source=researcher_app&utm_medium=referral&utm_campaign=RESR_MRKT_Researcher_inbound.

Schulz, S., Lichtmannegger, J., Schmitt, S., Leitzinger, C., Eberhagen, C., Einer, C., Kerth, J., Aichler, M., and Zischka, H. (2015). A protocol for the parallel isolation of intact mitochondria from rat liver, kidney, heart and brain. Methods Mol. Biol. *1295*, 75–86. https://doi.org/10.1007/978-1-4939-2550-6_7.

Schweppe, D.K., Eng, J.K., Yu, Q., Bailey, D., Rad, R., Navarrete-Perea, J., Huttlin, E.L., Erickson, B.K., Paulo, J.A., and Gygi, S.P. (2020). Full-featured, real-time database searching platform enables fast and accurate multiplexed quantitative proteomics. J. Proteome Res. *19*, 2026–2034. https://doi.org/10.1021/acs.jproteome.9b00860.

Shehata, M., Matsumura, H., Okubo-Suzuki, R., Ohkawa, N., and Inokuchi, K. (2012). Neuronal stimulation induces autophagy in hippocampal neurons that is involved in AMPA receptor degradation after chemical long-term depression. J. Neurosci. *32*, 10413–10422. https://doi.org/10.1523/JNEUROSCI.4533-11.2012.

Soubannier, V., Rippstein, P., Kaufman, B.A., Shoubridge, E.A., and McBride, H.M. (2012). Reconstitution of mitochondria derived vesicle formation demonstrates selective enrichment of oxidized cargo. PLoS One *7*, e52830. https://doi.org/10.1371/journal.pone.0052830.

Stavoe, A.K., Gopal, P.P., Gubas, A., Tooze, S.A., and Holzbaur, E.L. (2019). Expression of WIPI2B counteracts age-related decline in autophagosome biogenesis in neurons. Elife *8*, e44219. https://doi.org/10.7554/eLife.44219.

Strømhaug, P.E., Berg, T.O., Fengsrud, M., and Seglen, P.O. (1998). Purification and characterization of autophagosomes from rat hepatocytes. Biochem. J. *335*, 217–224. https://doi.org/10.1042/bj3350217.

Sugiura, A., McLelland, G.-L., Fon, E.A., and McBride, H.M. (2014). A new pathway for mitochondrial quality control: mitochondrial-derived vesicles. EMBO J *33*, 2142–2156. https://doi.org/10.15252/embj.201488104.

Szatmári, Z., Kis, V., Lippai, M., Hegedus, K., Faragó, T., Lorincz, P., Tanaka, T., Juhász, G., and Sass, M. (2014). Rab11 facilitates cross-talk between autophagy and endosomal pathway through regulation of Hook localization. Mol. Biol. Cell *25*, 522–531. https://doi.org/10.1091/mbc.E13-10-0574.

Tellez-Nagel, I., Johnson, A.B., and Terry, R.D. (1974). Studies on brain biopsies of patients with Huntington's chorea. J. Neuropathol. Exp. Neurol. *33*, 308–332. https://doi.org/10.1097/00005072-197404000-00008.

Truckenbrodt, S., Viplav, A., Jähne, S., Vogts, A., Denker, A., Wildhagen, H., Fornasiero, E.F., and Rizzoli, S.O. (2018). Newly produced synaptic vesicle proteins are preferentially used in synaptic transmission. EMBO J *37*, e98044. https://doi.org/10.15252/embj.201798044.

Tyanova, S., Temu, T., Sinitcyn, P., Carlson, A., Hein, M.Y., Geiger, T., Mann, M., and Cox, J. (2016). The Perseus computational platform for comprehensive analysis of (prote)omics data. Nat. Methods *13*, 731–740. https://doi.org/10.1038/nmeth.3901.

van Beek, N., Klionsky, D.J., and Reggiori, F. (2018). Genetic aberrations in macroautophagy genes leading to diseases. Biochim. Biophys. Acta Mol. Cell Res. *1865*, 803–816. https://doi.org/10.1016/j.bbamcr.2018.03.002.

Vincow, E.S., Thomas, R.E., Merrihew, G.E., Shulman, N.J., Bammler, T.K., MacDonald, J.W., MacCoss, M.J., and Pallanck, L.J. (2019). Autophagy accounts for approximately one-third of mitochondrial protein turnover and is protein selective. Autophagy *15*, 1592–1605. https://doi.org/10.1080/15548627.2019.1586258.

Wang, C., Ward, M.E., Chen, R., Liu, K., Tracy, T.E., Chen, X., Xie, M., Sohn, P.D., Ludwig, C., Meyer-Franke, A., Karch, C.M., Ding, S., and Gan, L. (2017). Scalable Production of iPSC-Derived Human Neurons to Identify Tau-Lowering Compounds by High-Content Screening. Stem Cell Reports *9*, 1221–1233. https://doi.org/10.1016/j.stemcr.2017.08.019.

Wong, Y.C., and Holzbaur, E.L.F. (2014). The regulation of autophagosome dynamics by huntingtin and HAP1 is disrupted by expression of mutant huntingtin, leading to defective cargo degradation. J. Neurosci. *34*, 1293–1305. https://doi.org/10.1523/JNEUROSCI.1870-13.2014.

Xie, Z., Bailey, A., Kuleshov, M.V., Clarke, D.J.B., Evangelista, J.E., Jenkins, S.L., Lachmann, A., Wojciechowicz, M.L., Kropiwnicki, E., Jagodnik, K.M., et al. (2021). Gene set knowledge discovery with Enrichr. Curr. Protoc. *1*, e90. https://doi.org/10.1002/cpz1.90.

Yu, C.H., Davidson, S., Harapas, C.R., Hilton, J.B., Mlodzianoski, M.J., Laohamonthonkul, P., Louis, C., Low, R.R.J., Moecking, J., De Nardo, D., et al. (2020). TDP-43 triggers mitochondrial DNA release via mPTP to activate cGAS/STING in ALS. Cell *183*, 636–649.e18. https://doi.org/10.1016/j.cell.2020.09.020.

Zellner, S., Schifferer, M., and Behrends, C. (2021). Systematically defining selective autophagy receptor-specific cargo using autophagosome content profiling. Mol. Cell *81*, 1337–1354.e8. https://doi.org/10.1016/j.molcel.2021.01.009.

Zhang, T., Shen, S., Qu, J., and Ghaemmaghami, S. (2016). Global analysis of cellular protein flux quantifies the selectivity of basal autophagy. Cell Rep *14*, 2426–2439. https://doi.org/10.1016/j.celrep.2016.02.040.

Zhang, X., Wang, T., Ji, J., Wang, H., Zhu, X., Du, P., Zhu, Y., Huang, Y., and Chen, W. (2020). The distinct spatiotemporal distribution and effect of feed restriction on mtDNA copy number in broilers. Sci. Rep. *10*, 3240. https://doi.org/10.1038/s41598-020-60123-1.

Please cite this article in press as: Goldsmith et al., Brain-derived autophagosome profiling reveals the engulfment of nucleoid-enriched mitochondrial fragments by basal autophagy in neurons, Neuron (2021), https://doi.org/10.1016/j.neuron.2021.12.029

STAR★METHODS

KEY RESOURCES TABLE

REAGENT or RESOURCE	SOURCE	IDENTIFIER
Antibodies		
LC3 Rabbit polyclonal antibody	Novus Biologicals	NB100-2220; RRID:AB_10003146
Synapsin I (for detection of mouse) Rabbit polyclonal antibody	EMD Millipore	Ab1543P; RRID:AB_90757
Synapsin I (for detection of human) Mouse monoclonal antibody	Synaptic Systems	106-011; RRID:AB_2619772
GM130 Mouse monoclonal antibody	BD Biosciences	610823; RRID:AB_398142
Histone H3 Rabbit polyclonal antibody	Cell Signaling Technology	9715; RRID:AB_331563
Calnexin Rabbit polyclonal antibody	Enzo life sciences	ADI-SPA-860-D; RRID:AB_2038898
Calreticulin Rabbit monoclonal antibody	Abcam	Ab92516; RRID:AB_10562796
Rab11A Rabbit polyclonal antibody	Zymed	71-5300; RRID:AB_2533987
Rab7 Mouse monoclonal antibody	Abcam	Ab50533; RRID:AB_882241
Rab5 Mouse polyclonal antibody	BD Biosciences	610281; RRID:AB_397676
EEA1 Mouse polyclonal antibody	BD Biosciences	610456; RRID:AB_397829
HSP60 Mouse monoclonal antibody	Enzo Life Sciences	SPA-806; RRID:AB_11177888
SOD1 Sheep polyclonal antibody	EMD Millipore	574597; RRID:AB_565164
SDHA Rabbit monoclonal antibody	Cell Signaling Technology	11998; RRID:AB_2750900
PHB2 Rabbit monoclonal antibody	Cell Signaling Technology	14085S; RRID:AB_2798387
Cytochrome c Mouse monoclonal antibody	Santa Cruz	Sc-13561; RRID:AB_627381
TOMM20 Mouse monoclonal antibody	Santa Cruz	Sc-17764 (F-10); RRID:AB_628381
TOMM40 Rabbit polyclonal antibody	Proteintech	18409-1-AP; RRID:AB_2303725
TOMM70 Rabbit polyclonal antibody	Proteintech	14528-1-AP; RRID:AB_2303727
Miro2 Rabbit polyclonal antibody	Proteintech	11237-1-AP;RRID:AB_2179539
P62/SQSTM1 Guinea Pig polyclonal antibody	American Research Products	03-GP62-C; RRID:AB_1542690
NDP52 Rabbit polyclonal antibody	Abcam	Ab68588; RRID:AB_1640255
NBR1 Mouse monoclonal antibody	Santa Cruz	Sc-130380; RRID:AB_2149402
VCP Rabbit polyclonal antibody	Cell Signaling Techonology	2648S; RRID:AB_2214632
Tax1bp1 Mouse monoclonal antibody	Santa Cruz	Sc-393143
OPTN Rabbit polyclonal antibody	Abcam	Ab23666; RRID:AB_447598
BNIP3 Mouse monoclonal antibody	Santa Cruz	Sc-56167; RRID:AB_2066767
PINK1 Mouse monoclonal antibody	Abcam	Ab75487; RRID:AB_1310581
Parkin Rabbit polyclonal antibody	Abcam	Ab15954; RRID:AB_443270
Nix Mouse monoclonal antibody	Santa Cruz	Sc-166332; RRID:AB_2066782
mtTFA (TFAM) (for detection in mouse) Rabbit monoclonal antibody	Abcam	Ab252432
TFAM (for detection in human) Rabbit polyclonal antibody	Abcam	Ab47517; RRID:AB_945799
GFP Chicken monoclonal antibody	Living color	632381; RRID:AB_2313808
Vamp2 Rabbit monoclonal antibody	Cell Signaling Technology	13508; RRID:AB_2798240
Synaptophysin Mouse monoclonal antibody	Enzo Life Sciences	VAM-8V011
Drp1 Mouse monoclonal antibody	Abcam	Ab56788; RRID:AB_941306
Fis1 Mouse monoclonal antibody	Santa Cruz	sc-376447; RRID:AB_11149382
Mff Mouse monoclonal antibody	Santa Cruz	Sc-398617; RRID:AB_2744543
Opa Mouse monoclonal antibody	Santa Cruz	Sc-393296
Mfn2 Mouse monoclonal antibody	Santa Cruz	Sc-515647; RRID:AB_2811176
GFAP Mouse monoclonal antibody	Cell Signaling Technology	3670S; RRID:AB_561049
Lamp1 Rat antibody	RDI	MCD107A-D4B

(*Continued on next page*)

Please cite this article in press as: Goldsmith et al., Brain-derived autophagosome profiling reveals the engulfment of nucleoid-enriched mitochondrial fragments by basal autophagy in neurons, Neuron (2021), https://doi.org/10.1016/j.neuron.2021.12.029

Continued

REAGENT or RESOURCE	SOURCE	IDENTIFIER
CD63 Rabbit monoclonal antibody	Abcam	Ab217345; RRID:AB_2754982
CHMP4b Rabbit polyclonal antibody	Proteintech	13683-1-AP; RRID:AB_2877971
HGS Rabbit polyclonal antibody	Abcam	Ab155539
STAM Mouse monoclonal antibody	Santa Cruz	Sc-133093; RRID:AB_2197486
Anti-Rabbit IgG-IRDye 800CW, Donkey Polyclonal	Licor	Cat# 926-32213; RRID: AB_621848
Anti-Rabbit IgG-IRDye 680RD, Donkey Polyclonal	Licor	Cat# 926-68073; RRID: AB_10954442
Anti-Mouse IgG-IRDye 800CW, Donkey Polyclonal	Licor	Cat# 926-32212; RRID: AB_621847
Anti-Mouse IgG-IRDye 680RD, Donkey Polyclonal	Licor	926-68072; RRID:AB_10953628
Anti-Guinea Pig IgG-IRDye 680RD, Donkey Polyclonal	Licor	926-68077; RRID:AB_10956079
Anti-Chicken IgG-IRDye 680RD, Donkey Polyclonal	Licor	926-68075; RRID:AB_10974977
Anti-Sheep IgG AlexaFluor 680, Donkey Polyclonal	Invitrogen	A-21102; RRID:AB_2535755
Chemicals, peptides, and recombinant proteins		
Lipofectamine 2000	Thermo Fisher	Cat# 11668019
SNAP-Cell 647-SiR	New England Biosciences	Cat# S9102S
PLL (mol wt 70,000 – 150,000)	Sigma-Aldrich	Cat# P1274
2.5% Trypsin	Thermo Fisher	Cat# 15090-046
Minimum essential medium (MEM)	Thermo Fisher	Cat# 11095-072
Horse serum (heat inactivated)	Thermo Fisher	Cat# 16050-122
Sodium Pyruvate	Corning	Cat# 36017004
D-Glucose solution 45%	Sigma-Aldrich	Cat# G8769
GlutaMAX	Thermo Fisher	Cat# 35050061
B27 Supplement	Thermo Fisher	Cat# 17504-044
Neurobasal medium	Thermo Fisher	Cat# 21103-049
Penicillin-Streptomycin	Thermo Fisher	Cat# 15140-122
AraC	Sigma-Aldrich	Cat# C6645
Matrigel Growth Factor Reduced	Corning	Cat# 354230
Essential 8 Medium	Thermo Fisher	Cat# A1517001
ReLeSR	StemCell Technologies, Inc.	Cat# 05872
Accutase	StemCell Technologies, Inc.	Cat# 07920
ROCK Inhibitor Y-27632	Selleckchem	Cat# S1049
DMEM/F12, HEPES	Thermo Fisher	Cat# 11330032
N2 Supplement	Thermo Fisher	Cat# 17502048
Nonessential Amino Acids	Thermo Fisher	Cat# 11140050
Doxycycline	Sigma-Aldrich	Cat# D9891
Poly-L-ornithine	Sigma-Aldrich	Cat# P3655
BrainPhys Neuronal medium	StemCell Technologies, Inc.	Cat# 05790
Laminin	Corning	Cat# 354232
BDNF	PeproTech	Cat# 450-02
NT-3	PeproTech	Cat# 450-03
OptiMEM	Gibco	2192535
Hibernate A	BrainBits	HALF
Hibernate E	BrainBits	HELF
Halt Protease and Phosphatase Inhibitor Cocktail	Thermo Fisher	Cat# 78442
Bradford reagent	Sigma	B6916
SDS (for proteomics)	Bio-Rad	Cat#1610302
TCEP	Gold Biotechnology	51805-45-9
Formic Acid	Sigma-Aldrich	Cat# C0267
Trypsin (for proteomics)	Promega	Cat# V511C

(*Continued on next page*)

Please cite this article in press as: Goldsmith et al., Brain-derived autophagosome profiling reveals the engulfment of nucleoid-enriched mitochondrial fragments by basal autophagy in neurons, Neuron (2021), https://doi.org/10.1016/j.neuron.2021.12.029

Continued

REAGENT or RESOURCE	SOURCE	IDENTIFIER
Rapigest SF Surfactant	Glixx Laboratories	Cat#GLXC-07089
EPPS	Sigma-Aldrich	Cat#E9502
2-Choroacetamide	Sigma-Aldrich	Cat#C0267
Empore SPE Disks C18	3M-Sigma-Aldrich	Cat#66883-U
Immobilon-FL PVDF membranes	Millipore	IPFL00010
Li-Cor Revert Total Protein Stain	Licor	926-11021
TrueBlack WB Blocking Buffer	Biotium	20T1021
TrueBlack WB Antibody Diluent	Biotium	23013B
SYBR Gold	Invitrogen	S11494
CellMask Deep Red	Invitrogen	C10046
MitoTracker Deep Red	Thermo Fisher	M22426
LysoTracker Deep Red	Thermo Fisher	L12492
Percoll	Sigma	Cat#P1644
Proteinase K	Sigma	Cat#P2308
Gly-Phe-Beta-naphthylamide	Cayman Chemical	Cat#14636
Nycodenz	Cosmo Bio USA	Cat#1002424
Optiprep	Cosmo Bio USA	Cat#04-03-9392/01
Critical commercial assays		
GFP-Trap Magnetic beads	ChromoTek	Gtd-10
Protein A dynabeads	Novex Life Technologies	10002D
Luna Universal qPCR master mix	New England Biolabs	M3003
Tandem Mass Tags	Thermo Fisher Scientific	Cat#90406
Bio-Rad Protein Assay Dye Reagent Concentrate	Bio-Rad	Cat#5000006
Experimental models: Cell lines		
i^3N iPSCs	Fernandopulle et al. (2018)	Gift from Dr. Michael Ward
Experimental models: Organisms/strains		
B6Cg-Tg(CAG-EGFP/LC3)53Nmi/NmiRbrc)	(Mizushima et al., 2004)	RIKEN BioResource Center in Japan
Oligonucleotides		
Primer: L1MdTf1 Forward: TTTGGGACACAATGAAAGCA Reverse: CTGCCGTCTACTCCTCTTGG	This paper	N/A
Primer: L1MdTf2 Forward: GCGAGGATGTGGAGAAAGAG Reverse: AGTTGGGGCTTCTTCTGGAT	This paper	N/A
Primer: ND2 Forward: ATCCTCCTGGCCATCGTACT Reverse: ATCAGAAGTGGAATGGGGCG	This paper	N/A
Primer: ND5 Forward: ACCCAATCAAACGCCTAGCA Reverse: AGGACTGGAATGCTGGTTGG	This paper	N/A
Primer: COXII Forward: AACCGAGTCGTTCTGCCAAT Reverse: CTAGGGAGGGGACTGCTCAT	This paper	N/A
Recombinant DNA		
Plasmid: EGFP-LC3	(Kabeya et al., 2000)	Addgene 21073
Plasmid: mCherry-Synapsin	This paper	N/A
Plasmid: mCherry vector	This paper	N/A
Plasmid: mito-dsRed	This paper	N/A
Plasmid: Snap-TFAM	This paper	N/A

(*Continued on next page*)

Please cite this article in press as: Goldsmith et al., Brain-derived autophagosome profiling reveals the engulfment of nucleoid-enriched mitochondrial fragments by basal autophagy in neurons, Neuron (2021), https://doi.org/10.1016/j.neuron.2021.12.029

Continued

REAGENT or RESOURCE	SOURCE	IDENTIFIER
Plasmid: mCherry-LC3	This paper	N/A
Plasmid: Cox8a-BFP	This paper	N/A
Plasmid: pGFP-Drp1	This paper	N/A
Plasmid: pGFP-Drp1K38A	This paper	N/A
Software and algorithms		
Enrichr	Xie et al. (2021)	https://maayanlab.cloud/Enrichr/
SynGO	Koopmans et al. (2019)	https://syngoportal.org/
FIJI	NIH, USA	https://imagej.net/Fiji
Perseus	Tyanova et al. (2016)	https://maxquant.net/perseus/
ImageStudio	Li-Cor	https://www.licor.com/bio/image-studio-lite/
Volocity	PerkinElmer	
Prism 9	GraphPad	https://www.graphpad.com/scientific-software/prism/
R	The R Foundation	https://www.r-project.org/
Mass spectrometry data analysis software	Huttlin et al. (2010)	N/A
Comet	(Eng et al., 2013)	http://comet-ms.sourceforge.net/
Other		
Biorender for model preparations	Biorender	https://biorender.com/
Sketch for figure preparation (v70.2)	Sketch	https://www.sketch.com/
Orbitrap Fusion Lumos Mass Spectrometer	ThermoFisher Scientific	Cat#IQLAAEGAAPFADBMBHQ
Easy-nLC 1200	ThermoFisher Scientific	LC140
Aeris™ 2.6 μm PEPTIDE XB-C18 100 Å 250 x 4.6 mm	Phenomenex	Cat#00G-4505-E0
Sep-Pak tC18 1cc Vac Cartridge, 50 mg	Waters	Cat#WAT054960
Empore™ SPE Disks C18	3M Bioanalytical Technologies	Cat# 2215

RESOURCE AVAILABILITY

Lead contact

Further information and requests for resources and reagents should be directed to and will be fulfilled by the lead contact, Erika Holzbaur (holzbaur@pennmedicine.upenn.edu).

Materials availability

Plasmids used in this study are available on request.

Data and code availability

- The full proteomic datasets reported here are included in the supplemental information (Table S1). All other data are available from the lead contact on request.
- No original code was generated in the course of this study.
- Any additional data or information required to reanalyze the data reported in this study is available from the lead contact on request.

EXPERIMENTAL MODEL AND SUBJECT DETAILS

Animal models

For mass spectrometry and immunoblotting analysis of brain-derived autophagic vesicles, wildtype and GFP-LC3B transgenic mice (strain: B6Cg-Tg(CAG-EGFP/LC3)53Nmi/NmiRbrc) generated by Mizushima et al. (2004) and available from RIKEN BioResource Center in Japan (PMID 14699058) of both sexes at 7–8 months of age were euthanized according to the University of Pennsylvania Institutional Animal Care and Use Committee approved procedures, and the brain above the brainstem was removed and homogenized in a sucrose buffer (see method details).

Please cite this article in press as: Goldsmith et al., Brain-derived autophagosome profiling reveals the engulfment of nucleoid-enriched mitochondrial fragments by basal autophagy in neurons, Neuron (2021), https://doi.org/10.1016/j.neuron.2021.12.029

Cell lines, primary cultures

Primary rat hippocampal neurons from E18 Sprague Dawley rats were purchased through the University of Pennsylvania Neuron Culture Service Center facility—the sex of the rats was not determined. Primary mouse cortical neurons were dissected and cultured in our laboratory. Briefly, E15.5 embryos from B6NTac (model #B6) mice were dissected, and the cortex was removed and dissociated with 0.25% trypsin and trituration. Neurons were plated in attachment media (MEM supplemented with 10% horse serum, 33 mM D-glucose and 1 mM sodium pyruvate) on poly-L-lysine coated 35 mm glass-bottom imaging dishes (P35G-1.5-20-C; MatTek). After 4–6 h, media was replaced with maintenance media (Neurobasal [GIBCO] supplemented with 2% B-27 [GIBCO], 33 mM D-glucose [Sigma], 2 mM GlutaMAX [GIBCO], 100 U/mL penicillin and 100 mg/mL streptomycin [Sigma]). AraC (1 μM) was added the day after plating to prevent glia cell proliferation. Every 3–4 days, 40% of the media was replaced with fresh Maintenance Media, and at DIV7-9, the neurons were used for imaging or biochemical analysis.

Human i^{3}N iPSCs that harbor a doxycycline-inducible mNGN2 transgene in the AAVS1 safe-harbor locus were a gift from Dr. Michael Ward (National Institutes of Health), and the characterization, culture, and differentiation protocols can be found (Fernando-pulle et al., 2018; Wang et al., 2017; Boecker et al., 2019). i^{3}Neurons differentiate with >90% efficiency into glutamatergic neurons . Briefly, iPSCs were cultured on Growth Factor Reduced Matrigel (Corning) in Essential 8 medium (Thermo Fisher). Cytogenetic analysis of G-banded metaphase cells demonstrated a normal male karyotype. Cells are periodically tested for mycoplasma. Differentiation into i^{3}Neurons was achieved by splitting the iPSCs with Accutase (Sigma) for a single cell suspension and plating on Matrigel-coated dishes in induction medium (DMEM/F12 supplemented with 2μg/mL doxycycline, 1% N2 supplement (Gibco), 1% nonessential amino acids (Gibco) and 1% GlutaMAX (Gibco). After three days, predifferentiated i^{3}Neurons were dissociated and plated onto poly-L-ornithine coated plates or imaging dishes at optimal densities. i^{3}Neurons were cultured in BrainPhys Neuronal Medium (StemCell) supplemented with 2% B27 (GIBCO), 10 ng/mL BDNF (PeproTech), 10 ng/mL NT-3 (PeproTech), and 1 μg/mL Laminin (Corning) for 21 days before experimentation. Every 3–4 days, 40% of the medium was carefully replaced with fresh culture medium. For each experiment, a biological replicate is defined as cells from different batches of inductions.

METHOD DETAILS

Isolation of autophagic vesicles by differential centrifugation

Enriched autophagosome fractions were isolated following a protocol modified from Strømhaug et al. (1998); (Maday and Holzbaur, 2014). Briefly, one mouse brain or ~30 million neurons were collected in a 250mM sucrose solution buffered with 10μM HEPES and 1mM EDTA at pH 7.3, homogenized using a tissue grinder, incubated with Gly-Phe-β-naphthylamide (GPN) for 7 min at 37°C to destroy lysosomes, and subsequently subjected to three differential centrifugations through 9.5% Nycodenz and 33% Percoll and 30% Optiprep discontinuous gradients to isolate vesicles of the appropriate size and density. After collection, the autophagic vesicle enriched fraction (AV) was divided into three, one third was treated with 10μg Proteinase K for 45min at 37°C, similar to Le Guerroué et al. (2017); Zellner et al. (2021) to degrade nonmembrane protected proteins and enrich for internal autophagosome cargo (AV+PK), one third was membrane permeabilized by the addition of 0.2% Triton X-100 before the same Proteinase K treatment as a negative control (AP+Tx+PK), and the other third was left untreated for identification of all internal and externally associated proteins on autophagosomes. AV-enriched fractions were subsequently used for mass spectrometry, electron microscopy, immunoblotting, and confocal microscopy. Step-by-step instructions and checklists are available upon request.

Crude mitochondrial fraction enrichment

Brain homogenate was split for AV fractionation, and a fraction was used for crude mitochondrial preparations based on the protocol from (Schulz et al., 2015; Soubannier et al., 2012). Briefly, samples were spun at 2000xg, 7000xg, and 8000xg sequentially for 15 min at 4°C.

Proteomics—sample preparation and digestion

The AV and AV+PK fractions from five independent mouse brain preparations, from 3 male and 2 female mice, were lysed with RIPA buffer (50 mM HEPES (pH 7.4), 150 mM NaCl, 1% sodium deoxycholate, 1% NP-40, 0.1% SDS, 2.5 mM MgCl2, 10 mM sodium glycerophosphate, 10 mM sodium biphosphate) containing 1 μg/ml aprotinin, 1 μg/ml leupeptin, 1 mM benzamidine, 1 mM AEBSF, and 1% final SDS. Lysates were sonicated on ice three times, followed by centrifugation (13000 rpm, 5 min). Protein concentration was measured by Bradford assay. Protein extracts (50 ug) were subjected to disulfide bond reduction with 5 mM TCEP (room temperature, 10 min) and alkylation with 25 mM chloroacetamide (room temperature, 20 min), followed by TCA precipitation before protease digestion. Samples were resuspended in 100 mM EPPS, pH 8.5 containing 0.1% RapiGest and digested at 37°C for 8 h with Trypsin at a 100:1 protein-to-protease ratio. Trypsin was then added at a 100:1 protein-to-protease ratio, and the reaction was incubated for 6 h at 37°C. After incubation, digestion efficiency of a small aliquot was tested. Tandem mass tag labeling of each sample was performed by adding 5 μl the 20 ng/μL stock of TMT reagent along with acetonitrile to achieve a final acetonitrile concentration of approximately 25% (v/v). After incubation at room temperature for 1 h, labeling efficiency of a small aliquot was tested, and the reaction was then quenched with hydroxylamine to a final concentration of 0.5% (v/v) for 15 min. The TMT-labeled samples were pooled together at a 1:1 ratio. The sample was vacuum centrifuged to near dryness, resuspended in 5% formic acid for 15 min, centrifuged at 10000×g for 5 minutes at room temperature, and subjected to C18 solid-phase extraction (SPE) (Sep-Pak, Waters).

Please cite this article in press as: Goldsmith et al., Brain-derived autophagosome profiling reveals the engulfment of nucleoid-enriched mitochondrial fragments by basal autophagy in neurons, Neuron (2021), https://doi.org/10.1016/j.neuron.2021.12.029

Proteomics—Off-line basic pH reversed-phase (BPRP) fractionation

Dried TMT-labeled sample was resuspended in 100 μl of 10 mM NH_4HCO_3 pH 8.0 and fractionated using BPRP HPLC (Paulo et al., 2016). Briefly, samples were offline fractionated over a 90-min run into 96 fractions by high pH reverse-phase HPLC (Agilent LC1260) through an aeris peptide xb-c18 column (Phenomenex; 250 mm x 3.6 mm) with mobile phase A containing 5% acetonitrile and 10 mM NH_4HCO_3 in LC-MS grade H_2O, and mobile phase B containing 90% acetonitrile and 10 mM NH_4HCO_3 in LC-MS grade H_2O (both pH 8.0). The 96 resulting fractions were then pooled in a noncontinuous manner into 24 fractions (as outlined in Supplementary Figure 5 of (Paulo et al., 2016)) and 12 fractions (even numbers) were used for subsequent mass spectrometry analysis. Fractions were vacuum centrifuged to near dryness. Each consolidated fraction was desalted via StageTip, dried again via vacuum centrifugation, and reconstituted in 5% acetonitrile, 1% formic acid for LC-MS/MS processing.

Proteomics—Liquid chromatography and tandem mass spectrometry

Mass spectrometry data were collected using an Orbitrap Fusion Lumos mass spectrometer, coupled to a Proxeon EASY-nLC1200 liquid chromatography (LC) pump (Thermo Fisher Scientific). Peptides were separated on a 100 μm inner diameter microcapillary column packed in house with ~35 cm of Accucore150 resin (2.6 μm, 150 Å, Thermo Fisher Scientific, San Jose, CA) with a gradient consisting of 5%–20% (0-70 min) and 20%–24% (70-80min) (ACN, 0.1% FA) over a total 90-min run at ~550 nL/min. For analysis, we loaded 1/8 of each fraction onto the column. To reduce ion interference compared with MS^2 quantification, each analysis used the Multi-Notch MS^3-based TMT method (McAlister et al., 2014), combined with newly implemented Real Time Search analysis software (Erickson et al., 2019; Schweppe et al., 2020). The scan sequence began with an MS^1 spectrum (Orbitrap analysis; resolution 120,000 at 200 Th; mass range 350−1400 m/z; automatic gain control (AGC) target 3×10^6; maximum injection time 50 ms). Precursors for MS^2 analysis were selected using a TopSpeed acquisition scheme of 3 sec/cycle. MS^2 analysis consisted of collision-induced dissociation (quadrupole ion trap analysis; Rapid scan rate; AGC 2.5×10^4; isolation window 0.7 Th; normalized collision energy (NCE) 35; maximum injection time 35 ms). Monoisotopic peak assignment was used, previously interrogated precursors were excluded using a dynamic window (150 s ± 7 ppm), and dependent scan was performed on a single charge state per precursor. After acquisition of each MS^2 spectrum, a synchronous-precursor-selection (SPS) API-MS^3 scan was collected on the top 10 most intense ions b or y-ions matched by the online search algorithm in the associated MS^2 spectrum (Erickson et al., 2019; Schweppe et al., 2020). MS^3 precursors were fragmented by high energy collision-induced dissociation (HCD) and analyzed using the Orbitrap (NCE 65; AGC 2.5×10^5; maximum injection time 200 ms, resolution was 50,000 at 200 Th).

Proteomics—Data analysis

Mass spectra were processed using a Comet-based (v2018.01 rev.2) software pipeline (Eng et al., 2013). Spectra were converted to mzXML and monoisotropic peaks were reassigned using Monocle (Rad et al., 2021). MS/MS spectra were matched with peptide sequencesusing the Comet algorithm along with a composite sequence database including all canonical entries from the *Mus musculus* Reference Proteome UniProt database (SwissProt – 2017-05), as well as an in-house curated list of contaminants. This database was concatenated with one composed of all protein sequences in the reversed order. Trypsin was used as the digestion enzyme, two missed cleavages were allowed, and the minimal peptide length was set to 7 amino acids. Searches were performed using a 20 ppm precursor ion tolerance for total protein level analysis. The recommended product ion parameters for ion trap ms/ms were used (1.0005 tolerance, 0.4 offset (mono masses), theoretical_fragment_ions = 1). TMT tags on lysine residues and peptide N termini (+229. 1629 Da) and carbamidomethylation of cysteine residues (+57.021 Da) were set as static modifications, whereas oxidation of methionine residues (+15.995 Da) was set as a variable modification. Peptide-spectrum matches (PSMs) were adjusted to a 1% false discovery rate (FDR), and PSM filtering was performed using a linear discriminant analysis, as described previously (Huttlin et al., 2010), although considering the following parameters: Comet Log Expect and Diff Seq. Delta Log Expect, missed cleavages, peptide length, charge state, and precursor mass accuracy. For protein-level comparisons, PSMs were identified, quantified, and collapsed to a 1% peptide false discovery rate (FDR) and then collapsed further to a final protein-level FDR of 1% (Savitski et al., 2015). Moreover, protein assembly was guided by principles of parsimony to produce the smallest set of proteins necessary to account for all observed peptides. For TMT-based reporter ion quantitation, we extracted the summed signal-to-noise (S:N) ratio for each TMT channel and found the closest matching centroid to the expected mass of the TMT reporter ion (integration tolerance of 0.003 Da). Proteins were quantified by summing reporter ion counts across all matching PSMs using in-house software, as described previously (Huttlin et al., 2010). PSMs with poor quality, MS^3 spectra with more than 5 TMT reporter ion channels missing, or isolation specificity less than 0.6, or with TMT reporter summed signal-to-noise ratio that were less than 200 or had no MS^3 spectra were excluded from quantification.

Protein quantification values were exported for further analysis in Microsoft Excel and Perseus (Tyanova et al., 2016), and statistical test and parameters used are indicated in the corresponding datasets.

Immunoblotting

Samples were lysed in RIPA buffer (50 mM Tris-HCl, 150 mM NaCl, 0.1% Triton X-100, 0.5% deoxycholate, 0.1% SDS, 2x Halt Protease and Phosphatase inhibitor, PMSF, Pepstatin A, TAME and Leupeptin), centrifuged at 18,000g for 20min to clear unlysed and membranaous fractions, and then the protein concentration was determined by Bradford assay. Proteins were resolved on 8%, 10%, 12%, or 15% SDS-PAGE gels, based on the size of proteins to be identified. Proteins were transferred to Immobilon-FL

PVDF membranes (Millipore) using a wet blot transfer system (BioRad). In total, 15% gels were transferred in buffer containing 20% methanol. Membranes were stained for total protein using Li-Cor Revert Total Protein Stain. After imaging, the total protein was destained, blocked for 1hr at RT with TrueBlack WB Blocking Buffer (Biotium), and incubated with primary antibodies diluted in TrueBlack WB antibody diluent + 0.2% Tween-20 overnight at 4°C. Membranes were washed three times in TBS+ 0.1% Tween-20 and incubated with secondary antibodies (1:20,000 dilution) in TrueBlack WB antibody diluent + 0.2% Tween-20 + 0.1% SDS for 1hr at RT. After three washes in TBS+ 0.1% Tween-20, membranes were imaged using the Odyssey CLx Infrared Imaging System (LI-COR), and quantification of protein levels was performed using ImageStudio (Li-Cor).

For quantification of immunoblot data, an independent biological replicate is defined as a separate brain or neuron differentiation preparation. Data were excluded if the total protein levels were unquantifiable.

GFP immunoprecipitation

25μl of GFPtrap or Protein A dynabeads were washed three times in buffer (10mM Tris pH 7.5, 150mM NaCl, 0.5mM EDTA), added to AV fraction samples containing protease and phosphatase inhibitors to a final volume of 500ul, and incubated on a rotator at 4°C for 1hr. Beads were subsequently washed three times in wash buffer and transferred to a new tube before boiling in 2x denaturing sample buffer. Independent biological replicates are defined as a separate brain homogenate AV preparation.

Transfection for live imaging

For all transfections, 0.3μg of each plasmid was combined with 12ul lipofectamine 2000 total in final vol of 300ul OptiMEM and left on neurons for 45min at 37°C in a 5% CO_2 incubator. mCherry-Synapsin coexpression with GFP-LC3 was expressed for 72h, whereas all other constructs were imaged after 48h. For Snap labeling, neurons expressing Snap-TFAM or a negative control (GFP transfected) were incubated with 100nM of Snap-Cell 647-SiR for 30min at 37°C in a 5% CO_2 incubator. After incubation, neurons were washed 3 times and equilibrated with complete neuron media for 30min at 37°C in a 5% CO_2 incubator. After three more washes, neurons were switched to imaging media and imaged immediately.

Neuron imaging was performed in low fluorescence Hibernate E (for primary neurons) or Hibernate A (for i3Neurons) medium (Brain Bits) supplemented with 2% B27 and 2mM GlutaMAX. Neurons were imaged in an environmental chamber at 37°C on a Perkin Elmer UltraView Spinning Disk Confocal system with a Nikon Eclipse Ti inverted microscope, using an Apochromat 100x 1.49 NA oil immersion objective. Images were acquired with a Hamamatsu EMCCD C9100-50 camera controlled using Volocity software. Axons were identified based on morphological parameters and imaging occurred in the mid- to distal-axon defined as greater than 200μm from the soma. Timelapse recordings were acquired at a frame rate of 2 frames per second for 5 minutes.

For quantification, an independent biological replicate is defined as a separate neuron preparation and transfection. Only neurons with moderate levels of fluorescent protein expression were imaged. For all kymographs, only trafficking AVs (movement > 10μm) in the mid- to distal- axon (>200 μm from soma) were quantified for analysis. For kymograph analysis, an average of 7 axons with 22 moving LC3 puncta per experiment were observed per experiment (axons per experiment: 7.05 ± 0.60 SEM, 25% Percentile = 4.75, 75% Percentile = 10; LC3 puncta per experiment: 22.45 ± 1.93 SEM, 25% Percentile = 15, 75% Percentile = 29.25).

Electron microscopy

AV fractions and brain homogenate fractions were pelleted and fixed with 2.5% glutaraldehyde, 2.0% paraformaldehyde in 0.1M sodium cacodylate buffer, pH 7.4, overnight at 4°C. Fixed samples were then transferred to the Electron Microscopy Resource Laboratory at the University of Pennsylvania, where all subsequent steps were performed. After buffer washes, the samples were post-fixed in 2.0% osmium tetroxide for 1 hr at room temperature and then washed again in buffer, followed by dH_2O. After dehydration through a graded ethanol series, the tissue was infiltrated and embedded in EMbed-812 (Electron Microscopy Sciences, Fort Washington, PA). Thin sections were stained with lead citrate and examined with a JEOL 1010 electron microscope fitted with a Hamamatsu digital camera and AMT Advantage image capture software. Regions of dense AVs were chosen for imaging. Biological replicates are defined as separate brain-derived AV preparations.

Immunofluorescence of AVs

AVs were prepared from wildtype or GFP-LC3 mouse brains and stained with 1:200,000 dilution of CMDR, 1:100,000 dilution of SYBRgold, 10nM of MitoTracker Deep Red, or 10nM of LysoTracker Deep Red. The samples were plated on coverslips with the addition of 0.2% methyl cellulose for 10 minutes in the dark before imaging to concentrate AVs at the coverslip surface. Independent biological replicates are considered to be different brain homogenate AV preparations. Randomly selected fields where AVs were stationary were used for quantification. All image analysis was performed on raw data. Images were prepared in FIJI, and contrast and brightness were adjusted equally to all images within a series. Quantification of the percent of SYBR+ puncta or GFP-LC3 puncta colocalized to CMDR (mean ± SEM) was performed using automated distanced-based colocalization (FIJI, coloc2).

AVs from GFP-LC3 transgenic mouse brains or wild-type mouse brains were immunoprecipitated using an anti-LC3 antibody. Briefly, the anti-LC3 antibody ab48394 at a 1:20 dilution fixed to a plasma cleaned coverslip with 0.5% nitrocellulose and blocked in 3%BSA for 30min. AVs stained with SYBRgold or CMDR at the dilutions used above were incubated at RT for 45min and washed

2× in PBS before imaging on the confocal microscope. Automated segmentation (FIJI, Weka Trainable Segmentation) was used to identify puncta before the colocalization analysis.

qPCR

Total brain and AV fraction samples from four independent biological replicates were DNA extracted using Trizol, and qPCR was performed using the Luna Universal qPCR master mix and protocol, with 50ng DNA and final primer concentration of 0.25μM. For each biological replicate, 3 technical replicates were performed. The plate reader and analysis was performed using the QuantStudio 3 Real-Time PCR System controlled by using QuantStudio Design and Analysis Software (Thermo Fisher Scientific).

QUANTIFICATION AND STATISTICAL ANALYSIS

Mitochondrial annotations and sublocalizations were performed using the MitoCarta2.0 and UniProt databases (Calvo et al., 2016).

GraphPad prism software (v9.1.0) was used for statistical analysis. The statistical test performed for all immunoblot analyses and kymograph quantification analyses is Ordinary one-way ANOVA with Šídák's multiple comparisons test or Kruskal-Wallis test with Dunnet's multiple comparison test for data not normally distributed. The statistical test for the median cargo score values of subgroups of organelles (Figures 3 and S2) is RM one way ANOVA with Dunnet's multiple comparison test. The statistical test for all of the individual cargo score values not averaged over biological replicate (Figures S3 and S5) is the Dunn Test, performed in R. Statistical tests used are indicated in the figure legends. Biological replicates (n), defined in the method details, are always displayed as individual data points, and the precision measures (mean ± SEM) are displayed. Significance was defined as a p value < 0.05, and where appropriate, directly reported in the figure. * $p < 0.05$, ** $p < 0.01$, *** $p < 0.001$, **** $p < 0.0001$. R (v4.0.4) was used for cargo score plots . See code availability statement for additional details. Enrichr (Chen et al., 2013; Kuleshov et al., 2016; Xie et al., 2021) and SynGO (Koopmans et al., 2019) were used to compute the p values of gene ontology term enrichment. Proteins with a cargo score greater than the median were input into the softwares – the p value calculation is dependent on Fisher's exact test and the q value displays the Benjamini-Hochburg multiple hypothesis testing correction. Enrichr precomputes a background expected rank for each term in the gene set library. Neither software takes into account the background protein expression levels in specific organs.